

Life and reproduction of titanosaurs: Isotopic hallmark of mid-palaeolatitude eggshells and its significance for body temperature, diet, and nesting

Léa Leuzinger^{a,*}, Stefano M. Bernasconi^b, Torsten Vennemann^c, Zoneibe Luz^c, Pierre Vonlanthen^d, Alexey Ulianov^d, Claudia Baumgartner-Mora^d, E. Martín Hechenleitner^{a,e}, Lucas E. Fiorelli^a, Pablo H. Alasino^{a,f}

^a Centro Regional de Investigaciones Científicas y Transferencia Tecnológica de La Rioja (CRILAR), Provincia de La Rioja, UNLaR, SEGEMAR, UNCa, CONICET, Entre Ríos y Mendoza s/n (5301), Anillaco, La Rioja, Argentina

^b Geological Institute, ETH Zürich, Sonneggstrasse 5, 8092 Zürich, Switzerland

^c Institute of Earth Surface Dynamics (IDYST), University of Lausanne, Géopolis building, CH-1015 Lausanne, Switzerland

^d Institute of Earth Sciences (ISTE), University of Lausanne, Géopolis building, CH-1015 Lausanne, Switzerland

^e Instituto de Biología de la Conservación y Paleobiología (IBICOPA), DACEFyN- UNLaR, 5300 La Rioja, Argentina

^f Instituto de Geología y Recursos Naturales, Centro de Investigación e Innovación Tecnológica, Universidad Nacional de La Rioja (INGeReN-CENIIT-UNLaR), Avenida Gobernador Vernet y Apóstol Felipe, 5300 La Rioja, Argentina

ARTICLE INFO

Keywords:

Titanosaur eggs
Stable isotopes
Clumped isotopes
Late Cretaceous
NW Argentina

ABSTRACT

Eggshells represent an important part of the fossil record of Titanosauria (Dinosauria – Neosauropoda) and their stable isotope compositions are valuable palaeoenvironmental proxies. A new set of conventional ($\delta^{18}\text{O}$ and $\delta^{13}\text{C}$) and clumped (Δ_{47}) stable isotope compositions of titanosaurian eggshells is presented, together with that of a bone and a single associated tooth, sampled in three Late Cretaceous nesting sites from La Rioja Province, NW Argentina. The preservation state of the fossils was first evaluated using optical and analytical techniques, such as transmitted light and optical cathodoluminescence (CL) microscopy, energy dispersive X-ray spectroscopy (EDX), and laser ablation-inductively coupled plasma-mass spectrometry (LA-ICP-MS). The isotopic compositions of the fossils were then compared to those of associated carbonate rocks and nodules, hydrothermal calcite and quartz, and those reported for eggshells from other nesting sites worldwide. This large, combined sample set allows us to define an isotopic hallmark ($\delta^{13}\text{C}_{\text{VPDB}} = -15$ to -11‰ ; $\delta^{18}\text{O}_{\text{VSMOW}} = 27$ to 33‰) typical for well-preserved mid-palaeolatitude titanosaurian eggshells. This hallmark is intended to identify the oological specimens best suited for palaeoenvironmental reconstructions, for instance in museum collection samples that may lack associated abiogenic materials such as host rocks. In addition, our isotopic data support that titanosaurs were animals with an elevated body temperature, mainly feeding on C3 plants, and reproducing under conditions more arid than the long-term average. The data are in excellent agreement with the isotopic data reported from other mid-palaeolatitude nesting sites around the world, indicating that titanosaurs needed similar environmental conditions to reproduce, regardless of the palaeogeographic location of their habitat. Finally, we raise the question whether titanosaurs experienced reproduction-related fasting, as noted for several extant vertebrates, and discuss the complexity of interpreting Δ_{47} -derived temperatures, despite very consistent bulk isotopic data.

* Corresponding author.

E-mail address: leuzinger.lea@gmail.com (L. Leuzinger).

¹ Current affiliation: Laboratorio de Paleontología de Vertebrados, IDEAN (CONICET), Departamento de Ciencias Geológicas, FCEN, Universidad de Buenos Aires, Intendente Güiraldes 2160, Ciudad Universitaria – Pabellón II, C1428EGA Ciudad Autónoma de Buenos Aires, Argentina.

<https://doi.org/10.1016/j.chemgeo.2021.120452>

Received 10 February 2021; Received in revised form 5 July 2021; Accepted 21 July 2021

Available online 25 July 2021

0009-2541/© 2021 Elsevier B.V. All rights reserved.

1. Introduction

Reproduction is an essential trait of vertebrates, and the reproductive strategy adopted by a given species can be decisive for its success or decline when facing environmental stress and/or inter-taxa competition. In the fossil record, eggs provide undisputed evidence of breeding activity and represent key snapshots of the animal's life, contrasting with the vast expanse of the geological timescale. Like other archosaurs, titanosaurian dinosaurs were oviparous and laid eggs (Chiappe et al., 1998), which, as in other amniotes, provided protection and a stable micro-environment that contained all the essential nutrients for the embryo to develop in a terrestrial realm (Nys and Guyot, 2011). Titanosaurian eggs are known from several nesting sites worldwide, usually in association with fluvial deposits that may have been lithified. Nesting sites have been found in palaeolatitudes between 10° and 45° (e.g., Folinsbee et al., 1970; Erben et al., 1979; Sarkar et al., 1991; Chiappe et al., 2003; Cojan et al., 2003; Kim et al., 2009; Bojar et al., 2010; Fiorelli et al., 2012; Hechenleitner et al., 2016b, 2020). They are an invaluable record for this clade, especially when skeletal remains are poorly preserved or absent. Resistance of the eggshells to diagenetic alteration is mainly due to a dense microstructure low in organic matter content (about 2 vol% vs. >17 vol% in dentine and ~25 vol% in bone; Hincke et al., 2012; Wang and Cerling, 1994). Additionally, the nesting strategy adopted by titanosaurs, which consists of burying the eggs into the substrate (Hechenleitner et al., 2015), plays a key protective role against transport, breakage and weathering.

Vertebrate hard tissues (including eggshells, teeth and bones) crystallise from body fluids that are derived from ingested water and food. Therefore, their oxygen ($\delta^{18}\text{O}$) and carbon ($\delta^{13}\text{C}$) stable isotope compositions largely reflect environmental cycles and climatic conditions (DeNiro and Epstein, 1976, 1978; Luz et al., 1984; Luz and Kolodny, 1985; Cerling and Harris, 1999; Kohn and Cerling, 2002; Koch, 2007), and more generally the palaeoenvironment in which the animals used to live. Since they form within a short period of time (days to weeks) (e.g., Tütken, 2011) in the distal part of the oviduct (Nys and Gautron, 2007), fossil eggs are of prime interest as they represent very specific environmental conditions prevailing during the reproduction period. The isotopic compositions of eggshells thus reflect the body temperature, diet and water assimilated by the female just before and during the production of the eggs. However, the use of the isotopic compositions measured in fossil remains as reliable palaeoenvironmental indicators requires careful evaluation of the preservation state of their mineralogical, chemical, and isotopic compositions. As alteration of isotopic compositions can be cryptic, i.e., without unequivocal changes in the primary mineralogy and biogenic structure of the fossil material (e.g., Araújo et al., 2013), reliable indicators are increasingly needed in this field. In this context, we propose here a new definition of the $\delta^{13}\text{C}$ and $\delta^{18}\text{O}$ isotopic compositions characteristic of well-preserved titanosaurian eggshells that may be used as a hallmark in future work.

Several isotopic studies on titanosaurian eggshells from Europe and Asia have been carried out over the last decades to determine the conditions best suited for the reproduction of this clade in South America, Europe and Asia (Folinsbee et al., 1970; Erben et al., 1979; Sarkar et al., 1991; Riera et al., 2013; Eagle et al., 2015). However, none has focused so far on the nesting sites known from NW Argentina (Fiorelli et al., 2012; Hechenleitner et al., 2016b, 2020). This study presents the stable isotope compositions of titanosaurian eggshells, as well as that of a single tooth and a bone, discovered in three nesting sites of La Rioja Province (NW Argentina). After a careful determination of the preservation state of the fossils, and hence, of their potential as palaeoenvironmental and physiological proxies, we used the best-preserved specimens to re-evaluate the thermoregulation strategies of titanosaurs and the palaeoenvironmental conditions prevailing during nesting and incubation. Comparison of our results with previous studies from other mid-palaeolatitude nesting sites worldwide indicates that the conditions required for the breeding of titanosaurs in NW Argentina

were very similar to those in other sites. We also speculate that limiting food resources for a sizable population of very large animals was likely a controlling factor for sedentariness, which further supports the idea that titanosaurs were breeding migrants.

2. Nesting sites and materials

2.1. Nesting sites

Three nesting sites – Sanagasta, Tama, and Quebrada de Santo Domingo – all located in La Rioja Province, NW Argentina (Fig. 1), have been investigated in detail. For a general description of the regional geology, the reader is referred to previous work (Ciccioli et al., 2005; Ezpeleta et al., 2006; Grellet-Tinner and Fiorelli, 2010; Fiorelli et al., 2012; Hechenleitner et al., 2016b; Limarino et al., 2016; Basilici et al., 2017; Hechenleitner et al., 2020).

The nesting site of Sanagasta is located in the pedogenised sandstone deposits in the northwesternmost part of the Los Llanos Fm, in the Sierras Pampeanas (Fiorelli et al., 2012). The egg-bearing levels were affected by extensive palaeohydrothermal activity evidenced by numerous carbonate and silicate deposits and precipitates, possibly originating from vents, geysers or discharge channels (Fiorelli et al., 2012). The fact that eggshells are systematically found in association with hydrothermal features, together with the very common occurrence of overly thick eggshells (which necessarily implies massive extrinsic dissolution before the young could hatch) led to the hypothesis that some titanosaurs used hydrothermal heat for egg incubation (cf. Grellet-Tinner and Fiorelli, 2010; Hechenleitner et al., 2018b). In this context, the unusual thickness of the eggshells can be viewed as an adaptive trait compensating for the strong dissolution of the outer shell under the acidic conditions prevailing in most hydrothermal environments where silica is deposited. An Early Cretaceous age for the Los Llanos Fm deposits in Sanagasta had first been proposed based on compositional similarities between the egg-bearing sedimentary rocks and hydrothermal veins found in granitoids and pegmatitic intrusions associated to the Gondwanan Cycle and the Sierras Pampeanas orogeny (Galindo et al., 1997; Fiorelli et al., 2012). However, recent microfossil dating in the nearby site of Tama (Carignano et al., 2013; de Sosa Tomas et al., 2017) suggests that a Late Cretaceous age is more likely (Hechenleitner et al., 2018a).

The nesting site of Tama is also located in the Los Llanos Fm, but in an area once dominated by an ephemeral braided river system subjected to strong seasonality, alternating long arid periods and short episodes of precipitation (Ezpeleta et al., 2006; Basilici et al., 2017). No evidence for the occurrence of a palaeohydrothermal system in Tama has been identified so far. Several studies have reported the existence of abundant vegetation grown in cumulative, poorly-developed paleosols (Inceptisols), and a typical Late Cretaceous Gondwanan vertebrate fauna (Fiorelli et al., 2016; Basilici et al., 2017). Fossil remains include in situ titanosaurian egg clutches, probably buried in dug-out holes or mounds for incubation (Hechenleitner et al., 2015, 2016b; Basilici et al., 2017). The identification of charophytes and ostracods in the nearby lacustrine deposits (Carignano et al., 2013; de Sosa Tomas et al., 2017) supports a Campanian-Maastrichtian age for the fossil-bearing levels.

The nesting site of Quebrada de Santo Domingo belongs to the Late Cretaceous Ciénaga del Río Huaco Fm, which consists of a reddish fine- to medium-grained sandstone succession deposited in a semi-arid, fluvio-lacustrine environment (Ciccioli et al., 2005; Limarino et al., 2016; Hechenleitner et al., 2020). Numerous titanosaurian egg clutches have been preserved in several levels of fine-grained sandstone corresponding to floodplain deposits, while semi-articulated titanosaurian skeletons can be found in coarser interbeds interpreted as crevasse splay deposits (Hechenleitner et al., 2020). The fossiliferous levels crop out on either side of the valley, even though they are topographically higher and more exposed to weathering in the south, while in the north, they are overlaid by several meters of sedimentary deposits. In this study, the site of

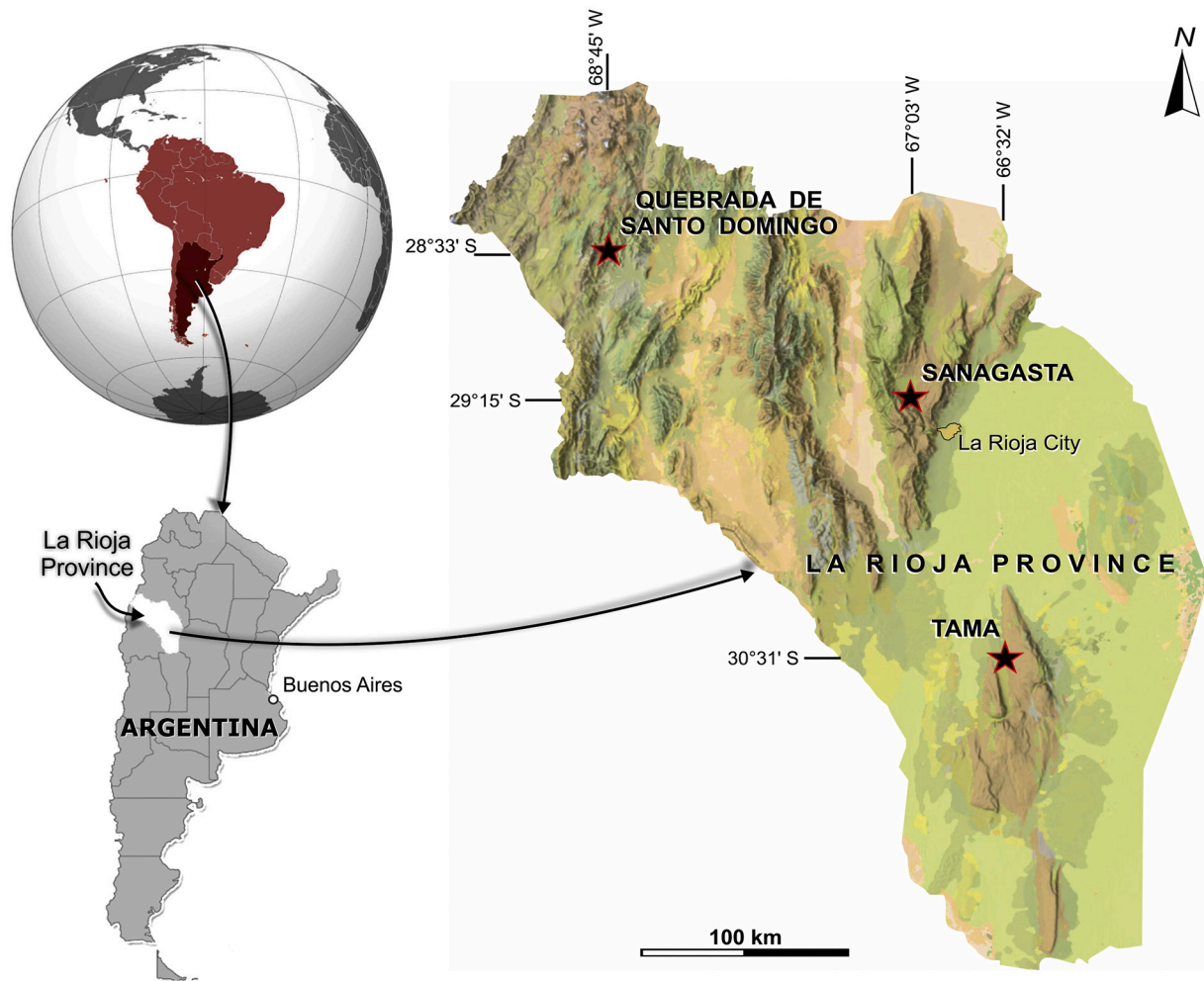


Fig. 1. Map showing the location of the three sites from which titanosaurian eggshells and skeletal remains have been collected.

Quebrada de Santo Domingo was divided into two subsites, abbreviated QSD Sur and QSD Norte hereafter. Eggshells were found in both subsites, while skeletal remains (including one tooth) were only excavated from QSD Sur. According to [van Hinsbergen et al. \(2015\)](#) and [Hechenleitner et al. \(2020\)](#), the Late Cretaceous palaeolatitude of Sanagasta, Tama and Quebrada de Santo Domingo, was between 32 and 35°S.

2.2. Materials

Several eggshell fragments from Sanagasta and Tama show large and sometimes translucent calcite and silica crystals, suggesting a significant degree of recrystallisation. Biogenic structures including shell units, radiating calcite crystals and pore canals are generally absent or clearly partly recrystallised as can be noted with a hand lens. In Quebrada de Santo Domingo, the general aspect of the eggshells is different in the two subsites. In QSD Sur, they are light greyish to white when freshly broken, and commonly cemented together. Some are heavily deformed and have lost their original gentle curvature. No biogenic structures can be distinguished, except the superficial ornamental features on the outer surface of the eggshells, suggesting a rather poor preservation state. In contrast, the eggshells from QSD Norte are dark gray to black in colour, and biogenic structures such as shell growth units are visible with a hand lens. When crushed, they release a strong hydrocarbon odour indicating a high volatile organic content, possibly unrelated to the original organic matter of the shells. The titanosaurian tooth found in association with a semi-articulated skeleton has translucent enamel, well distinguishable from the white dentine.

Seventy-one titanosaurian eggshell fragments, one bone and associated tooth, together with eighty-four abiogenic samples including bulk host sedimentary rocks, pedogenic and diagenetic carbonate nodules, hydrothermal calcite and quartz, and silicate clasts were collected (see [Table 1](#)). Eggshells, bulk sedimentary rocks, and carbonate nodules were sampled in the three nesting sites, while the hydrothermal crystals and the skeletal remains come from Sanagasta and QSD Sur, respectively. In [Table 1](#), eggshells with the same laboratory number but different letter (e.g., LL-82a, LL-82b) refer to samples from the same egg accumulation. The samples selected for stable isotope analyses are in the Palaeovertebrate Collection (Pv) repository of the Centro Regional de Investigaciones Científicas y Transferencia Tecnológica de La Rioja (CRILAR), Argentina.

3. Analytical techniques

The degree of preservation of the fossil remains, crucial for the interpretation of isotopic compositions, was evaluated using a combination of optical and in situ chemical analyses. The sample preparation followed a well-established procedure during which the fossil specimens were mounted in epoxy resin or cut in thin sections, stepwise diamond-powder polished down to a grade of 0.1 μm , and carbon coated to prevent charging. The samples intended for conventional and clumped stable isotope mass spectrometry were then prepared specifically. All the analytical work was carried out at the University of Lausanne (UNIL) and the Swiss Federal Institute of Technology (ETHZ), Zurich, Switzerland.

Table 1

$\delta^{13}\text{C}$ and $\delta^{18}\text{O}$ of titanosaurian SD and SE remains (eggshells and tooth), as well as associated abiogenic precipitates collected in the sites of Sanagasta, Tama, and Quebrada de Santo Domingo, NW Argentina.

Site	Sample type	Sample ID	Collection ID	$\delta^{13}\text{C}_{\text{CO}_3}$	$\delta^{18}\text{O}_{\text{CO}_3}$	SD	$\delta^{18}\text{O}_{\text{CO}_3}$	$\delta^{18}\text{O}_{\text{PO}_4}$	$\delta^{18}\text{O}_{\text{SiO}_2}$	$\delta^{18}\text{O}_{\text{H}_2\text{O}}^\dagger$	$\delta^{18}\text{O}_{\text{H}_2\text{O}}^\ddagger$		
				‰VPDB	‰VPDB		‰VSMOW	‰VSMOW	‰VSMOW	‰VSMOW	‰VSMOW		
Sanagasta	Eggshell	LL-114a	CRILAR-Pv 401	-9.3	-4.7	#	26.1	-	-	0.0	-		
		LL-114b	CRILAR-Pv 401	-9.5	-4.8	#	26.0	-	-	-0.1	-		
		LL-115a	CRILAR-Pv 401	-9.4	-5.0	0.1	25.8	-	-	-0.3	-		
		LL-115b	CRILAR-Pv 401	-8.4	-2.0	0.1	28.9	-	-	2.7	-		
		LL-116a	CRILAR-Pv-402	-8.6	-4.5	#	26.3	-	-	0.2	-		
		LL-116b	CRILAR-Pv-402	-8.0	-4.8	#	26.0	-	-	-0.1	-		
		LL-117a	CRILAR-Pv-402	-8.4	-4.1	0.1	26.7	-	-	0.6	-		
		LL-117b	CRILAR-Pv-402	-8.9	-4.1	#	26.7	-	-	0.7	-		
		LL-118a	CRILAR-Pv-403	-8.0	-3.9	#	26.9	-	-	0.8	-		
		LL-118b	CRILAR-Pv-403	-9.6	-1.1	0.1	29.8	-	-	3.6	-		
		LL-119a*	CRILAR-Pv-403	-8.3	-4.1	#	26.7	-	-	0.6	-		
		LL-121a	CRILAR-Pv-404	-8.5	-4.4	0.1	26.4	-	-	0.3	-		
		LL-121b	CRILAR-Pv-404	-9.0	-3.7	0.1	27.1	-	-	1.0	-		
		LL-122a	CRILAR-Pv-404	-8.7	-4.2	#	26.6	-	-	0.5	-		
		LL-122b*	CRILAR-Pv-404	-8.5	-5.2	#	25.6	-	-	-0.4	-		
		LL-123a	CRILAR-Pv-405	-9.2	-4.9	#	25.9	-	-	-0.1	-		
		LL-124a	CRILAR-Pv-405	-9.3	-5.1	#	25.7	-	-	-0.4	-		
		LL-124b	CRILAR-Pv-405	-8.7	-4.6	#	26.2	-	-	0.1	-		
		LL-124c	CRILAR-Pv-405	-9.3	-4.8	0.1	26.0	-	-	-0.1	-		
		LL-125	CRILAR-Pv-406	-8.8	-4.8	#	25.9	-	-	-0.1	-		
		LL-126	CRILAR-Pv-407	-9.2	-4.4	#	26.4	-	-	0.3	-		
		LL-126b	CRILAR-Pv-407	-8.8	-4.7	0.1	26.0	-	-	0.0	-		
		LL-127a	CRILAR-Pv-407	-8.8	-4.4	#	26.4	-	-	0.3	-		
		LL-127b	CRILAR-Pv-407	-9.5	-5.0	#	25.7	-	-	-0.3	-		
		LL-128b	CRILAR-Pv-408	-8.8	-5.1	#	25.6	-	-	-0.4	-		
		LL-129a	CRILAR-Pv-408	-9.1	-4.4	0.1	26.3	-	-	0.3	-		
		LL-130b*	CRILAR-Pv-409	-9.3	0.1	#	31.0	-	-	4.8	-		
		LL-131b	CRILAR-Pv-409	-7.6	-3.5	#	27.3	-	-	1.2	-		
			Sedimentary rock	SAN 3	-	-8.8	-6.1	#	24.6	-	-	-	-
				SAN 4	-	-7.8	-4.6	#	26.2	-	-	-	-
		SAN 5		-	-8.4	-5.2	#	25.6	-	-	-	-	
		SAN 6		-	-8.7	-4.2	#	26.6	-	-	-	-	
		SAN 8		-	-6.0	-8.2	#	22.4	-	-	-	-	
		SAN 9		-	-7.7	-7.9	#	22.7	-	-	-	-	
		SAN 11		-	-9.0	-4.8	#	26.0	-	-	-	-	
		SAN 12		-	-8.6	-4.3	#	26.5	-	-	-	-	
		SAN 13		-	-8.6	-4.8	#	26.0	-	-	-	-	
		SAN T1		-	-7.1	-4.6	#	26.2	-	-	-	-	
		SAN T2		-	-7.5	-4.7	#	26.1	-	-	-	-	
		SAN T3		-	-7.7	-4.7	#	26.1	-	-	-	-	
		SAN T4		-	-8.3	-5.0	#	25.8	-	-	-	-	
		SAN T5		-	-8.1	-4.7	#	26.1	-	-	-	-	
		SAN T6		-	-8.5	-4.8	#	26.0	-	-	-	-	
	SAN T7	-		-8.4	-4.5	#	26.2	-	-	-	-		
	Carbonate nodule	LL-174		-	-8.6	-5.1	#	25.7	-	-	-	-	
		LL-180*	-	-7.7	-4.9	#	25.9	-	-	-	-		
	Hydrothermal calcite	LL-48	-	-7.9	-4.9	#	25.9	-	-	-	-		
		LL-49	-	-7.5	-5.5	0.1	25.2	-	-	-	-		
		LL-50	-	-9.3	-7.0	#	23.7	-	-	-	-		
		LL-58	-	-9.1	-5.1	#	25.7	-	-	-	-		
		LL-61a	-	-8.4	-5.8	#	24.9	-	-	-	-		
		LL-61b	-	-8.4	-6.1	#	24.6	-	-	-	-		
		LL-61c	-	-9.1	-5.5	#	25.2	-	-	-	-		
		LL-61d	-	-9.5	-5.7	#	25.1	-	-	-	-		
		LL-61e	-	-9.6	-5.7	#	25.0	-	-	-	-		
		LL-62*	-	-9.4	-7.4	#	23.3	-	-	-	-		
		LL-98	-	-7.1	-4.8	#	25.9	-	-	-	-		
		LL-99	-	-7.9	-5.7	#	25.1	-	-	-	-		
		LL-100*	-	-8.0	-6.1	#	24.7	-	-	-	-		
		LL-101	-	-7.9	-4.8	#	26.0	-	-	-	-		
		LL-173a	-	-7.9	-4.7	#	26.1	-	-	-	-		
		LL-173b	-	-9.2	-7.9	#	22.8	-	-	-	-		
	LL-173c*	-	-7.9	-6.1	0.1	24.6	-	-	-	-			
	LL-173d	-	-8.8	-5.5	#	25.2	-	-	-	-			
	LL-173e	-	-8.4	-5.4	#	25.3	-	-	-	-			
	LL-175b*	-	-9.2	-5.9	#	24.8	-	-	-	-			
	LL-175c	-	-9.2	-5.6	#	25.1	-	-	-	-			
	LL-175d	-	-9.6	-5.6	#	25.1	-	-	-	-			
	LL-175f	-	-8.3	-7.6	#	23.1	-	-	-	-			
	LL-177a	-	-7.7	-4.8	#	25.9	-	-	-	-			
	LL-177c	-	-8.1	-5.9	#	24.9	-	-	-	-			
	LL-177e	-	-7.6	-5.2	#	25.5	-	-	-	-			

(continued on next page)

Table 1 (continued)

Site	Sample type	Sample ID	Collection ID	$\delta^{13}\text{C}_{\text{CO}_3}$ ‰VPDB	$\delta^{18}\text{O}_{\text{CO}_3}$ ‰VPDB	SD	$\delta^{18}\text{O}_{\text{CO}_3}$ ‰VSMOW	$\delta^{18}\text{O}_{\text{PO}_4}$ ‰VSMOW	$\delta^{18}\text{O}_{\text{SiO}_2}$ ‰VSMOW	$\delta^{18}\text{O}_{\text{H}_2\text{O}}^\dagger$ ‰VSMOW	$\delta^{18}\text{O}_{\text{H}_2\text{O}}^\ddagger$ ‰VSMOW
		LL-177f	-	-9.4	-8.0	#	22.7	-	-	-	-
		LL-178b	-	-8.9	-7.9	0.1	22.8	-	-	-	-
		LL-178c	-	-8.9	-5.4	#	25.3	-	-	-	-
		LL-178d	-	-9.5	-5.4	0.1	25.4	-	-	-	-
		LL-179b	-	-10.0	-6.2	#	24.6	-	-	-	-
	Hydrothermal quartz	LL_49	-	-	-	-	-	-	30.5	-	-
		LL_52	-	-	-	-	-	-	31.5	-	-
		LL_56	-	-	-	-	-	-	33.9	-	-
		LL_51	-	-	-	-	-	-	33.8	-	-
	Silicate clast	LL_50	-	-	-	-	-	-	30.5	-	-
		LL_75	-	-	-	-	-	-	10.7	-	-
		LL_73	-	-	-	-	-	-	12.7	-	-
		LL_53	-	-	-	-	-	-	13.3	-	-
		LL_48	-	-	-	-	-	-	11.6	-	-
		LL_77	-	-	-	-	-	-	11.1	-	-
Site	Sample type	Sample ID	Collection ID	$\delta^{13}\text{C}_{\text{CO}_3}$ ‰VPDB	$\delta^{18}\text{O}_{\text{CO}_3}$ ‰VPDB	$\delta^{18}\text{O}_{\text{CO}_3}$ ‰VSMOW	$\delta^{18}\text{O}_{\text{PO}_4}$ ‰VSMOW	$\delta^{18}\text{O}_{\text{SiO}_2}$ ‰VSMOW	$\delta^{18}\text{O}_{\text{H}_2\text{O}}^\dagger$ ‰VSMOW	$\delta^{18}\text{O}_{\text{H}_2\text{O}}^\ddagger$ ‰VSMOW	
		LL-109c	Pv-530/5 4c	-8.3	-5.1	25.6	-	-	-0.4	-	
		LL-110b	Pv-530/3 4bn1	-8.6	-4.9	25.9	-	-	-0.1	-	
		LL-110c	Pv-530/3 4bn1	-8.7	-4.6	26.2	-	-	0.1	-	
		LL-111a	Pv-530/4 4a	-8.8	-5.2	25.6	-	-	-0.4	-	
		LL-111b	Pv-530/4 4a	-9.0	-4.9	25.9	-	-	-0.2	-	
		LL-111c	Pv-530/4 4a	-8.6	-4.4	26.4	-	-	0.4	-	
		LL-170	N2F1i	-8.8	-5.7	25.1	-	-	-0.9	-	
	Sedimentary rock	N2F1	-	-9.2	-6.0	24.7	-	-	-	-	
		TAM 1	-	-9.1	-5.6	25.1	-	-	-	-	
		TAM 3	-	-9.1	-5.8	25.0	-	-	-	-	
		TAM 4	-	-9.0	-5.4	25.3	-	-	-	-	
	Carbonate nodule	LL-97*	-	-9.7	-5.9	24.8	-	-	-	-	
QSD Sur	Eggshell	LL-102a	CRILAR-Pv-621	-5.6	-0.7	30.2	-	-	4.1	-	
		LL-102b	CRILAR-Pv-621	-5.7	-0.5	30.4	-	-	4.3	-	
		LL-102c	CRILAR-Pv-621	-5.6	-0.2	30.7	-	-	4.5	-	
		LL-103a	CRILAR-Pv-621	-5.8	0.1	31.1	-	-	4.9	-	
		LL-103b	CRILAR-Pv-621	-3.7	-1.1	29.8	-	-	3.6	-	
		LL-103c	CRILAR-Pv-621	-5.3	1.7	32.7	-	-	6.5	-	
		LL-104a	CRILAR-Pv-621	-4.1	-2.6	28.2	-	-	2.1	-	
		LL-104b	CRILAR-Pv-621	-3.4	-0.4	30.5	-	-	4.4	-	
		LL-104c	CRILAR-Pv-621	-3.9	-2.4	28.5	-	-	2.4	-	
		LL-105a*	CRILAR-Pv-621	-5.6	-0.6	30.3	-	-	4.1	-	
		LL-105b	CRILAR-Pv-621	-6.2	-0.9	29.9	-	-	3.8	-	
		LL-105c	CRILAR-Pv-621	-5.8	0.6	31.5	-	-	5.3	-	
		LL-106	CRILAR-Pv-621	-2.9	-1.6	29.3	-	-	3.1	-	
		LL-107a	CRILAR-Pv-621	-6.1	-0.6	30.3	-	-	4.2	-	
		LL-107b	CRILAR-Pv-621	-6.4	-0.6	30.3	-	-	4.1	-	
		LL-107c	CRILAR-Pv-621	-6.4	-0.9	30.0	-	-	3.8	-	
		LL-83a	CRILAR-Pv-621	-5.4	-2.2	28.7	-	-	2.6	-	
		LL-83b	CRILAR-Pv-621	-5.1	-2.0	28.9	-	-	2.8	-	
		LL-84c	CRILAR-Pv-621	-4.4	-1.6	29.3	-	-	3.2	-	
		LL-86	CRILAR-Pv-621	-6.5	-0.2	30.7	-	-	4.5	-	
		LL-88a	CRILAR-Pv-621	-3.4	-1.9	28.9	-	-	2.8	-	
		LL-88b	CRILAR-Pv-621	-4.7	-2.1	28.8	-	-	2.6	-	
	Tooth enamel	LL-167,79	CRILAR-Pv-613	-7.6	-4.6	26.2	18.9	-	0.2	1.0	
	Tooth dentine	LL-168,80	CRILAR-Pv-613	-8.6	-7.5	23.2	16.9	-	-2.8	-0.9	
	Bulk tooth	LL-215	CRILAR-Pv-613	-7.7	-6.4	24.3	17.6	-	-1.7	-0.3	
	Bone	LL-218	CRILAR-Pv-613	-	-	-	16.6	-	-	-	
	Sedimentary rock	QSD 2	-	-6.6	1.9	32.9	-	-	-	-	
		QSD 3	-	-6.2	-2.6	28.2	-	-	-	-	
		QSD 8	-	-2.4	-2.3	28.6	-	-	-	-	
	Carbonate nodule	LL-85a	-	-6.9	6.7	37.8	-	-	-	-	
		LL-85b	-	-6.9	6.1	37.2	-	-	-	-	
		LL-85c	-	-6.9	6.3	37.4	-	-	-	-	
		LL-85d	-	-6.9	6.4	37.5	-	-	-	-	
		LL-85e*	-	-6.9	6.5	37.6	-	-	-	-	
		LL-85f	-	-6.8	6.3	37.4	-	-	-	-	
		LL-85 g	-	-6.9	6.5	37.6	-	-	-	-	
		LL-85 h*	-	-6.9	5.9	37.0	-	-	-	-	
		LL-85i	-	-6.9	5.8	36.9	-	-	-	-	
QSD Norte	Eggshell	LL-108a	CRILAR-Pv-620	-12.1	1.4	32.4	-	-	6.2	-	
		LL-108b*	CRILAR-Pv-620	-11.8	-0.7	30.2	-	-	4.0	-	
		LL-108c*	CRILAR-Pv-620	-8.7	-0.8	30.1	-	-	4.0	-	
		LL-108d	CRILAR-Pv-620	-12.0	1.2	32.1	-	-	5.9	-	
		LL-108e	CRILAR-Pv-620	-11.4	0.5	31.4	-	-	5.2	-	

(continued on next page)

Table 1 (continued)

Site	Sample type	Sample ID	Collection ID	$\delta^{13}\text{C}_{\text{CO}_3}$ ‰VPDB	$\delta^{18}\text{O}_{\text{CO}_3}$ ‰VPDB	$\delta^{18}\text{O}_{\text{CO}_3}$ ‰VSMOW	$\delta^{18}\text{O}_{\text{PO}_4}$ ‰VSMOW	$\delta^{18}\text{O}_{\text{SiO}_2}$ ‰VSMOW	$\delta^{18}\text{O}_{\text{H}_2\text{O}}^\dagger$ ‰VSMOW	$\delta^{18}\text{O}_{\text{H}_2\text{O}}^\ddagger$ ‰VSMOW
		LL-108f	CRILAR-Pv-620	-12.7	0.3	31.2	-	-	5.0	-
		LL-108 g*	CRILAR-Pv-620	-9.9	-0.5	30.4	-	-	4.3	-
		LL-82a	CRILAR-Pv-620	-12.2	1.0	32.0	-	-	5.8	-
		LL-82b	CRILAR-Pv-620	-12.4	1.1	32.0	-	-	5.8	-
		LL-82c	CRILAR-Pv-620	-12.0	0.9	31.9	-	-	5.7	-
		LL-82d*	CRILAR-Pv-620	-12.8	1.6	32.5	-	-	6.3	-
		LL-82e	CRILAR-Pv-620	-12.5	1.1	32.1	-	-	5.9	-
		LL-82f*	CRILAR-Pv-620	-11.9	0.3	31.2	-	-	5.0	-
	Sedimentary rock	QSD 4	-	-7.3	-4.0	26.8	-	-	-	-
		QSD 5	-	-7.1	-3.8	27.0	-	-	-	-
	Carbonate nodule	LL-81a*	-	-9.4	-2.6	28.2	-	-	-	-
		LL-81c	-	-9.0	-3.6	27.3	-	-	-	-
		LL-81d	-	-8.9	-2.9	27.9	-	-	-	-
		LL-81 g*	-	-8.8	-2.4	28.4	-	-	-	-
		LL-81 h	-	-9.2	-3.4	27.4	-	-	-	-
		LL-81j	-	-8.9	-2.8	28.0	-	-	-	-

* Samples selected for clumped stable isotope analyses (see Table 2).

† Calculated for body water using the calcite-water fractionation equation of Kim and O'Neil (1997) with T = 37 °C.

‡ Calculated for body water using the phosphate-water fractionation equation of Lécuyer et al. (2013) with T = 37 °C.

3.1. Optical methods

Eggshell thin sections were examined in transmitted and polarised light using a Leica DM 4500 P LED petrographic microscope equipped with an integrated digital camera. Optical examination and imaging was used to characterise features of interest and help constrain the samples of choice for further optical and analytical studies.

Optical cathodoluminescence (CL) images were taken on polished surfaces using Technosyn 8200 MkII unfocussed, cold cathode luminescope at a voltage of 15–20 kV and a current of 0.4–0.6 mA. The luminescope was mounted on an Olympus light microscope equipped with a static stage and a high-sensitivity Olympus DP74 camera. The images were taken in air but depressurised to 0.2 Torr (about 26.6 Pa). In calcite, a yellow-orange CL colour ($\lambda = 600\text{--}650\text{ nm}$) usually results from the incorporation of Mn^{2+} (20–1000 ppm) in the crystal lattice. In contrast, a dark bluish CL colour ($\lambda = 410\text{--}430\text{ nm}$) corresponds to the intrinsic luminescence of high-purity calcite, while violet-mauve CL colours ($\lambda = 380\text{--}410\text{ nm}$) arise from the combination of intrinsic luminescence and low (<20 ppm) Mn^{2+} content (Sommer, 1972; Baumgartner-Mora and Baumgartner, 1994). The quenching effect of Fe^{2+} was not considered here, as it requires high concentrations (in the thousands of ppm range) and is absent in (at least avian) eggshells (Bravo et al., 2003). The CL colours observed from tooth enamel are complex to decipher as they result from the combined effects of luminescence in calcite and hydroxyapatite, which are caused by both extrinsic chemical elements and structural defects. Nevertheless, a dark blue CL colour ($\lambda = 390\text{--}410\text{ nm}$) is generally accepted as a reliable indicator of high-purity and good preservation of biogenic hydroxyapatite (e.g., Götze, 2012).

3.2. In situ chemical analyses

Major and minor element concentrations were measured by energy-dispersive X-ray spectroscopy (EDX) using a Tescan Mira II LMU field emission-scanning electron microscope (FE-SEM) operated at an acceleration voltage of 20 kV, a probe current of 1.1 nA, and equipped with a PentaFETx3 Si(Li) X-ray detector controlled by the AZtec 2.4 software package. Backscattered electron (BSE) images (providing grayscale compositional contrast) were taken using the same instrument to highlight the different phases of the samples and spot the regions of interest for EDX analyses.

Rare Earth Element (REE) concentrations were measured by laser ablation-inductively coupled plasma-mass spectrometry (LA-ICP-MS). The data were acquired in two separate sessions using an Element XR

sector-field ICP mass spectrometer (ThermoFisher Scientific), interfaced to an UP-193 FX 193 nm excimer ablation system (ESI) during the first session, and linked to a RESolution 193 nm ESI equipped with an S155 two-volume ablation cell (ASI) during the second session. The reference material (NIST-SRM612) from the National Institute of Standards and Technology (NIST) was systematically analysed from four ablation spots in each series of measurements. The data were initially processed with the LamTrace (Lotus 1-2-3 spreadsheet) software (Jackson, 2008). It must be noted that LA-ICP-MS analyses of REE are commonly used to check the preservation state of biogenic hydroxyapatite. Rare Earth Elements are present in extremely low amount in biomineralised tissues of living organisms (<ppm, e.g., Kocsis et al., 2010), but they are easily incorporated into the hydroxyapatite lattice during diagenesis (Kohn and Cerling, 2002). Thus, the relative concentration of REE in hydroxyapatite can be very helpful to recognise provenance, reworking and recrystallisation (Henderson et al., 1983; Trueman et al., 2006; Tütken, 2011; Fadel et al., 2015). In contrast, the use of LA-ICP-MS analyses is unusual to check for the preservation state of carbonated fossil remains. However, its application was justified in the case of the eggshells from QSD Sur and QSD Norte in order to determine whether the striking difference in the degree of alteration observed in the hand-specimens and thin sections was supported by distinct REE compositions.

3.3. Stable isotope mass spectrometry

Carbon and oxygen stable isotope analyses ($\delta^{13}\text{C}$, $\delta^{18}\text{O}$, and Δ_{47}) of all types of carbonates (eggshells, bulk sedimentary rocks, nodules and hydrothermal calcite), except the structural carbonate in tooth hydroxyapatite were analysed according to the method described in Schmid and Bernasconi (2010) and refined by Meckler et al. (2014) and Müller et al. (2017). The outer and inner surfaces of the eggshells were removed using a Dremel 3000 rotary device, ultrasonically cleaned in distilled water, air-dried, and crushed into fine powder in an agate mortar. The same procedure was applied to the hydrothermal calcite and the carbonate nodules, in which the sampling was selectively limited to the central parts. For sedimentary rocks, the largest silicate clasts were handpicked and the matrix crushed into fine powder without any pre-treatment. The powder of each sample was then weighed into glass vials and analysed in a GasBench II system coupled to a ThermoFisher Scientific Delta V isotope ratio mass spectrometer at the Geology Institute of ETHZ. Tooth enamel and dentine, as well as bone tissues were collected separately with a rotary device, and the oxygen and carbon isotopic compositions of the structural carbonates in the

hydroxyapatite were measured at UNIL in a GasBench II system coupled to a Finnigan MAT Delta Plus XL mass spectrometer. The instruments of ETHZ and UNIL laboratories were calibrated against the international carbonate standard NBS-19 (TS limestone). Additionally, the isotopic compositions of in-house Carrara marble standards were measured together with the samples for data correction. The analytical precision of the analyses was better than $\pm 0.1\%$ for both carbon and oxygen isotope compositions.

For clumped isotope analyses (Δ_{47}), eggshells and hydrothermal calcite were sampled following the procedure described above. The amount of sample material to be weighed (equivalent to 100–120 μg of pure carbonate) was estimated based on the carbonate yield of each sample calculated from previous GasBench analyses. Between fifteen and twenty replicates were measured for individual eggshells ($n = 9$) and two to fourteen replicates for hydrothermal calcite ($n = 4$). The eggshell specimens were selected for Δ_{47} measurement according to the $\delta^{13}\text{C}$ and $\delta^{18}\text{O}$ values obtained from the GasBench measurements, that is two samples with average $\delta^{13}\text{C}$ and $\delta^{18}\text{O}$ values, and one outlier. The process consisted in reacting the powder with 104% phosphoric acid (Burman et al., 2005) at 70 °C in a ThermoFisher Scientific Kiel IV carbonate device linked to a MAT 253 mass spectrometer. The data correction procedure includes several steps, i.e., a pressure base-line correction (PBL), a transfer to an absolute reference frame and a correction for the phosphoric acid fractionation at 70 °C (for more detail, see Dennis et al., 2011; Bernasconi et al., 2013; Meckler et al., 2014). Raw data were processed with the community software “Easotope” (John and Bowen, 2016). Δ_{47} values were normalized to the CDES and to 25 °C acid reaction temperature according to Bernasconi et al. (2018). Temperatures were calculated with the Kele et al. (2015) equation as recalculated by Bernasconi et al. (2018).

Phosphate samples, i.e., dentine and enamel hydroxyapatite, were crushed into fine powders (2 mg each) and pre-treated following the procedure of Koch et al. (1997). The phosphate ions (PO_4^{3-}) were isolated as described in O’Neil et al. (1994) and precipitated as silver phosphate (Ag_3PO_4). The international standard NBS-120c (phosphorite: 21.7%) as well as the two in-house reference materials GW-1 and KHM-25 (great white shark tooth: 22.1%, and sea cow rib: 20.1%, respectively) were processed the same way as the samples for quality control. For each sample, three silver capsules containing 350–500 μg of Ag_3PO_4 powder were analysed at UNIL in a high-temperature conversion elemental analyser (TC/EA) coupled to a Finnigan MAT Delta Plus XL mass spectrometer (see Vennemann et al., 2002). Additionally, two in-house phosphate standards (LK-2 L: 12.1% and LK-3 L: 17.9%) that had better than $\pm 0.3\%$ standard deviations were used for data correction.

Silicate clasts and hydrothermal quartz (five each) were ultrasonically cleaned in distilled water and air-dried. The powder drilled out from the crystal bulk was then cleared from any carbonate residue in a 10 vol% HCl solution, rinsed several times with distilled water, and oven-dried at a temperature of 40 °C. The oxygen stable isotope composition of the samples (1–2 mg each) was analysed at UNIL with a CO_2 -laser fluorination line coupled to a Finnigan-MAT 253 mass spectrometer according to the method described in Lacroix and Vennemann (2015).

The reproducibility for $\delta^{13}\text{C}$ and $\delta^{18}\text{O}$ measurements were smaller than 0.1‰ for carbonate samples and tooth phosphates (enamel and dentine), and 0.2‰ for the bone phosphates. We obtained a value of $21.5 \pm 0.2\%$ for the standard NBS-120c, i.e., in agreement with the value of 21.7‰ typically considered for this standard (O’Neil et al., 1994). The Δ_{47} results and derived temperatures are presented with their standard error, and the temperatures with the 95% confidence interval. The accepted value for the internal quartz standard LS1 was of 18.1‰ on the VSMOW scale and this was measured with a precision of $\pm 0.1\%$.

4. Results

4.1. Fossil preservation

Thin section optical microscopy of the eggshells from Sanagasta, Tama and QSD Sur confirms poor preservation and massive recrystallisation (mainly silicates with minor secondary calcite), as observed macroscopically. The eggshells show extensive alteration features, with only occasional and partial preservation of biogenic structures. In contrast, the eggshells from QSD Norte show obvious biogenic features typical for the clade and indicative of good preservation. Those include a mono-layered shell structure, concentric wavy lines parallel to the shell surface (possibly related to organic matter incorporated during mineralisation; Williams and Vickers-Rich, 1992), and spherulites from which calcite fans nucleate and radiate to form shell units and superficial nodes (Fig. 2). Between the shell units, the pores ensuring gas exchange between the embryo and the outer environment are easily identifiable, even though most of them are filled with secondary calcite.

The CL images support the occurrence of different preservation states between the eggshells from Sanagasta, Tama and QSD Sur on one hand, and those from QSD Norte (Fig. 2) on the other hand. Bright yellow-orange (600 nm) CL colours are observed to varying degrees in the outer and inner rims and around spherulites and pores of the eggshells from all nesting sites. This likely results from the incorporation of Mn^{2+} in the calcite crystals under reducing diagenetic conditions (Sommer, 1972; Baumgartner-Mora and Baumgartner, 1994). This CL is concentrated in the outer and inner surfaces, especially around the spherulites, as well as along the pores. The concentric lines visible in thin section in QSD Norte eggshells are highlighted by bright yellow luminescence suggesting the metabolic or diagenetic incorporation of Mn^{2+} , while the zones in-between have a dark-blueish (410–430 nm) CL colour, typical for high-purity calcite and denoting a mostly Mn^{2+} -free shell volume.

In situ EDX chemical analyses further support calcite as being the main component of well-preserved eggshells from QSD Norte, while quartz is predominant in the eggshells from all the other sites (Fig. 3). Barite, a common mineral in hydrothermal or highly evaporative settings, has been identified in the eggshells from Sanagasta (and in the nearby sedimentary rocks; see Fiorelli et al., 2012) and, to a lesser extent, QSD Sur. Other allochthonous minerals trapped in the pore infill or heavily altered zones of the eggshells, and originating from the surrounding detritic sedimentary rocks, include Ti-rich Fe oxides in Sanagasta and Tama, plagioclase in Tama and QSD Sur, and unidentified V, Nd and Ce-bearing phases in QSD Norte.

LA-ICP-MS analyses of the eggshells from the two subsites of Quebrada de Santo Domingo have distinct REE patterns (Fig. 4A). In QSD Sur, the REE patterns are flat, with values between 0.1 and 1 when normalized against the North American Shale Composite (NASC) standard (a compilation of samples intended to represent an average composition of continental detrital rocks; see Gromet et al., 1984), indicating pervasive recrystallisation and alteration of the original biogenic material. In contrast, the eggshells from QSD Norte have much lower REE concentrations, between 0.001 and 0.1 when normalized against NASC (30 ng/g in total), suggesting a limited diagenetic overprint. The variations between neighbouring chemical elements are small (e.g., Tm = 4 ng/g, Yb = 6 ng/g, Lu = 2 ng/g).

With average concentrations of 9.4 $\mu\text{g/g}$ ($X_{\min} = 1.6 \mu\text{g/g}$, $X_{\max} = 20.7 \mu\text{g/g}$) and 26.1 $\mu\text{g/g}$ ($X_{\min} = 7.1 \mu\text{g/g}$, $X_{\max} = 51.9 \mu\text{g/g}$) for enamel and dentine, respectively, the overall content of REE in the titanosaurian tooth from QSD Sur is globally low, but one to two orders of magnitude higher than that reported for the eggshells (Fig. 4A). The higher REE concentrations measured in dentine compared to enamel is likely related to the higher porosity of the former, which makes incorporation of REE during recrystallisation easier (e.g., Kohn and Cerling, 2002; Kocsis et al., 2007, 2010). The REE patterns are typically bell-shaped, i.e., with substantial MREE-enrichment and low HREE and LREE values, a feature classically considered to be an indicator of extensive recrystallisation

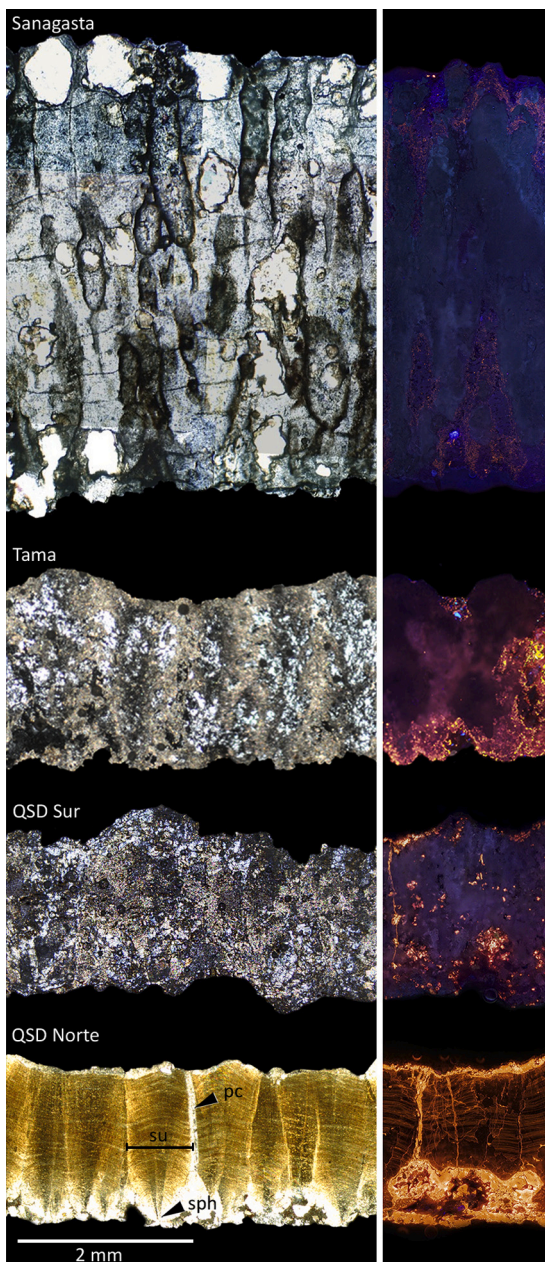


Fig. 2. Transmitted light thin section (left) and CL (right) images showing the outstanding preservation state of titanosaurian eggshells from QSD Norte compared to the heavily recrystallised specimens from Sanagasta, Tama, and QSD Sur. The bright yellow-orange CL colours results from the incorporation of Mn^{2+} in the calcite crystals under reducing diagenetic conditions. Dark blue (410–430 nm) CL colours are interpreted here as primary calcite lacking Mn^{2+} . Violet-mauve colours arise from the combination of intrinsic CL and low Mn^{2+} activation. Note that the most commonly observed preservation state is shown here and that less severely recrystallised eggshells have been used for taxonomic identification (see Fig. 5 in Grellet-Tinner and Fiorelli, 2010, and Fig. 6 in Hechenleitner et al., 2016b). QSD = Quebrada de Santo Domingo; pc = pore canal; sph = spherulite; su = shell unit. (For interpretation of the references to colour in this figure legend, the reader is referred to the web version of this article.)

during late diagenesis (e.g., Reynard et al., 1999; Lécuyer et al., 2003; Trueman et al., 2006). More recent studies, however, have shown that it may also result from REE fractionation (Kocsis et al., 2010; Mackenzie et al., 2011; Fadel et al., 2015). Here, the relatively low total REE content together with the dark blue CL colour (Fig. 4B) suggest that tooth

enamel has preserved its primary biomineral composition and that the bell shape of the REE patterns likely results from fractionation rather than diagenetic processes.

4.2. Stable isotope compositions

Conventional carbon and oxygen isotope compositions ($\delta^{13}C$ and $\delta^{18}O$) are listed in Table 1 and plotted in Fig. 5. Clumped (Δ_{47}) isotope compositions and calculated precipitation temperatures (T , °C) are listed in Table 2.

The eggshells from Sanagasta ($n = 28$) have $\delta^{13}C$ values within the narrow range of -9.6 to -7.6 ‰, with an average ($\delta^{13}C_{av}$) of -8.8 ± 0.5 ‰. The $\delta^{18}O$ values are between 25.5 and 27.3 ($\delta^{18}O_{av} = 26.6 \pm 1.3$ ‰), except for three “outliers” (LL-115b, LL-118b, LL-130b) with values of 28.9‰, 29.8‰ and 30.6‰ respectively. The Δ_{47av} value ($n = 3$) is 0.642 ± 0.007 ‰ ($T = 34.8 \pm 5.8$ °C). The eggshells from Tama ($n = 8$) have very similar $\delta^{13}C$ and $\delta^{18}O$ values to those from Sanagasta, ranging from -9.0 to -8.3 ‰ ($\delta^{13}C_{av} = -8.7 \pm 0.2$ ‰) and 25.1 to 26.4‰ ($\delta^{18}O_{av} = 25.8 \pm 0.4$ ‰), respectively. No Δ_{47} was measured on the eggshells from Tama. The eggshells from the two subsites of Quebrada de Santo Domingo have different isotopic compositions, especially in their carbon isotopic composition. With $\delta^{13}C$ values ranging between -6.5 and -2.9 ‰ ($\delta^{13}C_{av} = -5.1 \pm 1.1$ ‰), the eggshells from QSD Sur ($n = 22$) have the highest $\delta^{13}C$ values measured in this study. Conversely, with a $\delta^{13}C_{av}$ value of -11.7 ± 1.4 ‰ (between -12.8 and -8.7 ‰), the eggshells from QSD Norte ($n = 13$) have the lowest $\delta^{13}C_{av}$ value. The stable oxygen isotope compositions are not markedly different between the two subsites, with $\delta^{18}O$ values from 28.2 to 32.7‰ ($\delta^{18}O_{av} = 30.0 \pm 1.1$ ‰) and from 30.1 to 32.5‰ ($\delta^{18}O_{av} = 31.5 \pm 1.2$ ‰) for QSD Sur and QSD Norte, respectively. Those results are, however, notably higher than those reported for the eggshells from Tama and Sanagasta. The Δ_{47av} value is 0.597 ± 0.007 ‰ ($T = 50.7 \pm 6.0$ °C) for the eggshells from QSD Norte ($n = 5$, 16 to 20 replicates each), and 0.755 ± 0.006 ‰ ($T = 3.3 \pm 3.8$ °C) for the single eggshell measured from QSD Sur (18 replicates). In all sites, we observe obvious differences in the $\delta^{18}O$ and $\delta^{13}C$ values (up to 3‰ and 4‰, respectively) for the eggshells belonging to the same egg accumulation (i.e., same laboratory number but different letter, see Table 1).

The bulk sedimentary rocks ($n = 16$) and hydrothermal calcite ($n = 12$) from Sanagasta have $\delta^{13}C$ and $\delta^{18}O$ values in the range of -10.0 to -6.0 ‰ ($\delta^{13}C_{av} = -8.4 \pm 0.8$ ‰) and 22.4 to 26.6‰ ($\delta^{18}O_{av} = 25.1 \pm 1.1$ ‰), respectively. Some $\delta^{18}O$ values are marginally lower in hydrothermal calcite compared to sedimentary rocks, but no such trend is observed in the $\delta^{13}C$ values. The Δ_{47av} value of hydrothermal calcite ($n = 4$) is 0.635 ± 0.003 ‰ ($T = 36.6 \pm 6.8$ °C). The $\delta^{18}O$ values of the silicate clasts ($n = 5$) and of hydrothermal quartz ($n = 5$) differ substantially from each other, with values of 10.7 to 13.3‰ ($\delta^{18}O_{av} = 11.9 \pm 1.1$ ‰) for the former and 30.5 to 33.9‰ ($\delta^{18}O_{av} = 32.0 \pm 1.7$ ‰) for the latter. Isotopic compositions for the bulk sedimentary rocks in Tama ($n = 4$) cluster even more tightly, with $\delta^{13}C$ values in the range of -9.2 to -9.0 ‰ ($\delta^{13}C_{av} = -9.1 \pm 0.1$ ‰) and $\delta^{18}O$ values between 24.7 and 25.3‰ ($\delta^{18}O_{av} = 25.0 \pm 0.3$ ‰). The sedimentary rocks from Quebrada de Santo Domingo ($n = 5$) show a wide spread of isotopic compositions, with $\delta^{13}C$ values between -7.3 and -2.4 ‰ ($\delta^{13}C_{av} = -5.9 \pm 2.0$ ‰) and $\delta^{18}O$ values from 26.8 to 32.9‰ ($\delta^{18}O_{av} = 28.7 \pm 2.5$ ‰), the lower values for both $\delta^{13}C$ and $\delta^{18}O$ being those from QSD Norte.

The pedogenic carbonate nodules from Sanagasta ($n = 2$) have $\delta^{13}C$ values of -8.6 and -7.7 ‰ ($\delta^{13}C_{av} = -8.2 \pm 0.0$ ‰) and $\delta^{18}O$ values of 25.7 and 27.0‰ ($\delta^{18}O_{av} = 26.4 \pm 0.0$ ‰). In Tama ($n = 1$), $\delta^{13}C$ and $\delta^{18}O$ values are -9.7 ‰ and 24.8‰, respectively. In QSD Sur ($n = 9$), $\delta^{13}C$ values of diagenetic nodules are surprisingly close to each other, between -6.9 and -6.8 ‰ ($\delta^{13}C_{av} = -6.9 \pm 0.0$ ‰), while $\delta^{18}O$ values are the highest reported in this study, with values topping between 36.9 and 37.8‰ ($\delta^{18}O_{av} = 37.4 \pm 0.3$ ‰). In QSD Norte ($n = 6$), $\delta^{13}C$ and $\delta^{18}O$ values are in the range of -9.4 to -8.8 ‰ ($\delta^{13}C_{av} = -9.0 \pm 0.2$ ‰), and 27.3 to 28.4‰ ($\delta^{18}O_{av} = 27.9 \pm 0.4$ ‰) for diagenetic nodules,

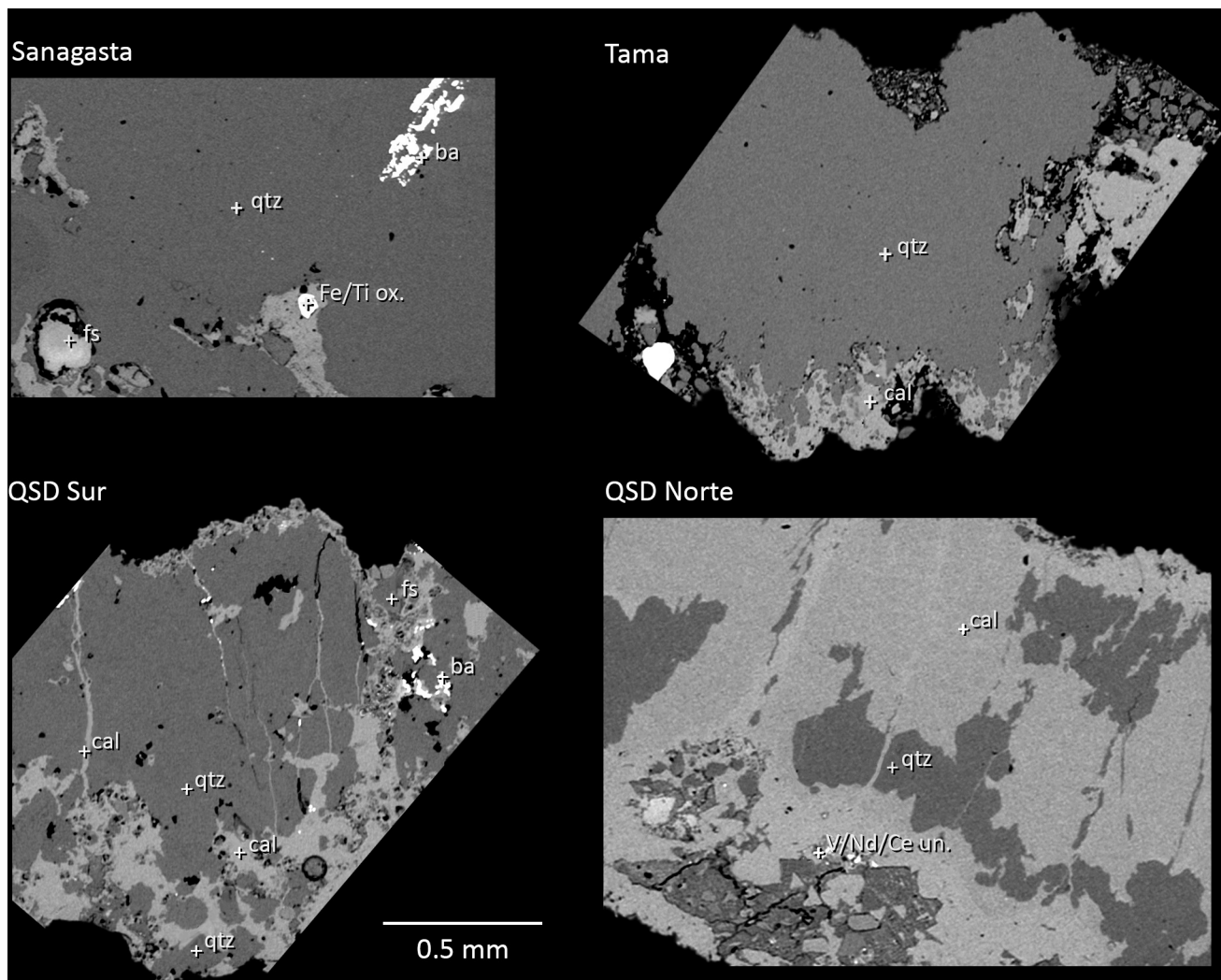


Fig. 3. SEM BSE images showing the typical mineral phases identified by EDX analyses in titanosaurian eggshells. Note the difference in the amount of quartz and calcite between QSD Norte and the other sites. QSD = Quebrada de Santo Domingo; ba = barite; cal = calcite; fs = feldspar; qtz = quartz; Ti/Fe ox. = Ti-rich Fe oxide; V/Nd/Ce un. = unidentified V, Nd and Ce-bearing phases.

respectively. The Δ_{47av} values of the nodules are $0.622 \pm 0.005\%$ ($T = 40.5 \pm 6.7$ °C) in QSD Sur ($n = 2$) and $0.626 \pm 0.008\%$ ($T = 40.2 \pm 6.5$ °C) in QSD Norte ($n = 2$).

Hydroxyapatite from the titanosaurian skeletal remains has $\delta^{18}O_{PO_4}$ values of 18.9‰ for enamel, 16.9‰ for dentine and 16.6‰ for the bone. The structural carbonate of the enamel has a $\delta^{13}C_{CO_3}$ value of -7.6% and a $\delta^{18}O_{CO_3}$ value of 26.2‰, while that of dentine has corresponding values of -8.6% and 23.2‰.

5. Discussion

5.1. The isotopic composition of well-preserved eggshells and tooth

5.1.1. Associated abiogenic geological samples as comparative tools

A common way of identifying potential disturbances of the biogenic isotopic composition is to compare the data provided by the best-preserved fossils with the results obtained from the matrix and the other associated abiogenic materials (carbonate rocks and nodules, hydrothermal calcite and quartz). Fractionation processes involved in the formation of biogenic vs. abiogenic material may be different (physiological vs. physicochemical). Also, the crystallisation temperature and the source of carbon often differ between biogenic and abiogenic materials. Therefore, an overlap of the isotopic compositions measured in

the biogenic and abiogenic materials is commonly regarded as evidence for pervasive diagenesis of the fossil sample and poor preservation of the original biogenic isotopic composition (e.g., Riera et al., 2013). Conversely, an offset in the isotopic compositions between fossils and associated abiogenic samples is to be expected when diagenetic processes are absent or limited in extent.

Most freshwater carbonates have $\delta^{13}C$ values between -5 and $+5\%$ (Clark and Fritz, 1997; Kelly, 2000). In contrast, the $\delta^{13}C$ values recorded in the hard tissues of herbivorous vertebrates are lower, since carbon is sourced from the ingested plants, which preferentially fix ^{12}C from atmospheric CO_2 during photosynthesis (e.g., Farquhar et al., 1989). Consequently, well-preserved eggshells are expected to have lower $\delta^{13}C$ values than the associated, inorganically precipitated materials. Regarding oxygen, the $\delta^{18}O$ values measured in minerals mainly reflect the water source and the temperature of formation. Depending on the mechanism at play, $\delta^{18}O$ values can have a very broad range, but usually below the upper bound of $\sim 29\%$ in abiogenic freshwater carbonates (Nelson and Smith, 1996). In vertebrate biominerals (e.g., $CaCO_3$ or $Ca_{10}(PO_4)_6(OH)_2$), however, physiological fractionation processes such as water loss through evapotranspiration (Koch, 2007; Lazzarini et al., 2016) may also come into play, making body water (and tissues) typically enriched in ^{18}O compared to meteoric (ingested) water (Koch, 2007). In the case of vertebrates, the precipitation temperature of

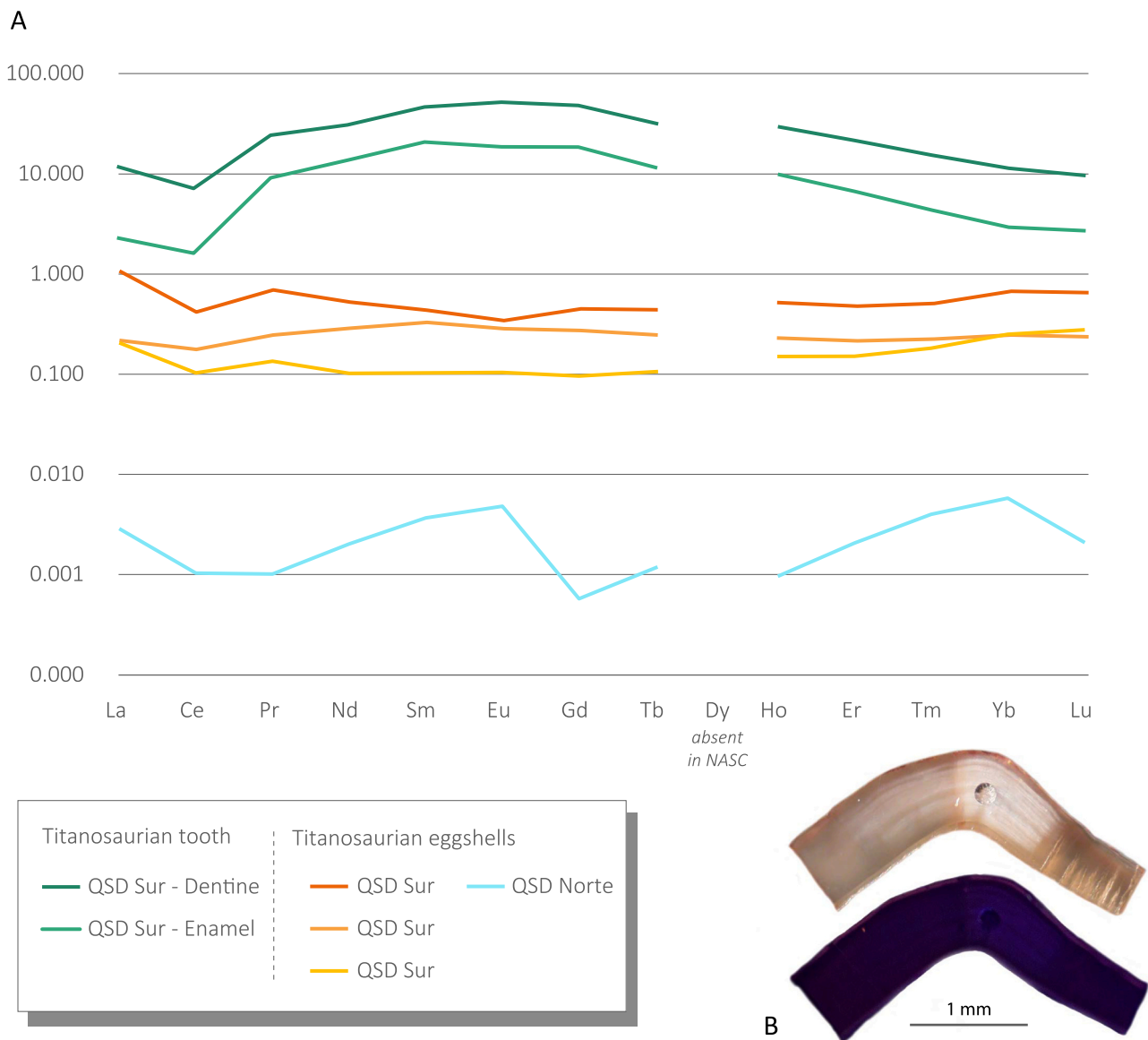


Fig. 4. (A) LA-ICP-MS REE concentrations of the titanosaurian eggshells and the tooth from Quebrada de Santo Domingo (QSD), normalized against NASC; (B) polished section (top) and CL imaging (bottom) of a QSD Sur titanosaurian tooth enamel fragment (section perpendicular to the growth axis). The ablation crater indicates the location of the LA-ICP-MS spot. Note the presence of growth lines in the polished section.

biomineralised tissues, recorded in their $\delta^{18}\text{O}$ values, corresponds to the animal's body temperature, which can be higher than (common in mammals and birds), or similar to (in most reptiles and fish) the ambient air, respectively water, temperature. As a first approximation, we can thus expect higher $\delta^{18}\text{O}$ values for well-preserved eggshells than for the associated abiogenic geological samples, assuming that both are related to the same source of (meteoric) water and have formed at similar temperatures. However, if body temperatures were higher than ambient air temperatures, the $\delta^{18}\text{O}$ values will be lower than the values expected for the mineral-water equilibrium under ambient conditions.

Most of the eggshells from Sanagasta and Tama (Los Llanos Fm) show evidence for extensive recrystallisation and poor preservation (if any) of the original biogenic structures (see Section 4.1.). Not surprisingly, their $\delta^{13}\text{C}$ and $\delta^{18}\text{O}$ values reflect neither the environmental conditions, nor the physiological processes occurring during the lifetime of the dinosaurs, but mainly the temperatures and oxygen isotopic composition prevailing during diagenesis. This also applies to the Δ_{47} values of the eggshells from Sanagasta, which do not reflect primary conditions either. At most, the slightly higher $\delta^{18}\text{O}$ values (Fig. 5) noted in the

eggshells than in the associated pedogenic carbonate nodules and sedimentary rocks (25.1 to 27.3‰ for most eggshells and 22.4 to 26.6‰ for abiogenic material) might be interpreted as partial or even complete preservation of primary values. The three supposedly better-preserved eggshells from Sanagasta (see “outliers” in Fig. 5), with clearly higher $\delta^{18}\text{O}$ values (28.9, 29.8 and 31.0‰) than all the other samples from the Los Llanos Fm, support this hypothesis.

The eggshells from the two subsites of Quebrada de Santo Domingo (Ciénaga del Río Huaco Fm) have different results compared to the host rock material. The isotopic compositions of the eggshells from QSD Sur – considered to be poorly preserved (see Section 4.1.) – are widely scattered, and are more similar to the sedimentary rock from QSD than the eggshells of Sanagasta and Tama (Los Llanos Fm, Fig. 5). The diagenetic carbonate nodules from QSD Sur clearly differ from the sedimentary rock and eggshells in their $\delta^{18}\text{O}$, which is surprisingly high. We suggest that these nodules formed relatively recently under evaporative surface conditions in arid settings resulting in high $\delta^{18}\text{O}$ values (e.g., Koch et al., 2003). The presence of gypsum veins in the egg-bearing levels, as well as barite in some eggshells (see Fig. 3) support the presence of warm

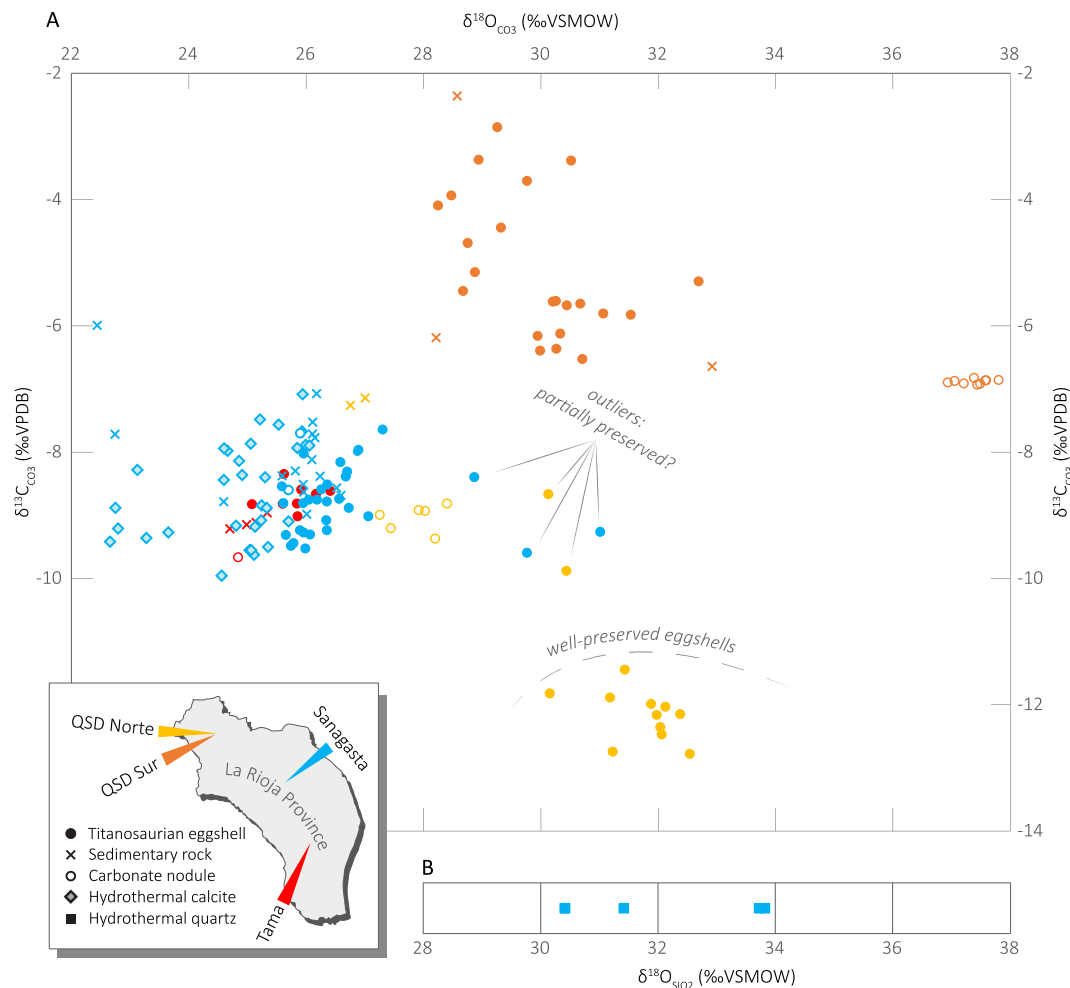


Fig. 5. Carbon and oxygen stable isotope composition of (A) carbonate samples, showing the strong clustering of the well-preserved eggshells from QSD Norte compared to their associated, abiogenic geological samples and to the eggshells from the other nesting sites of La Rioja, NW Argentina, and (B) silicate samples indicating a hydrothermal/meteoric origin. Silicate clasts of magmatic origin ($\delta^{18}\text{O} = 10.7$ to 13.3‰) are not shown. QSD = Quebrada de Santo Domingo.

diagenetic fluids, as do the Δ_{47} values measured in the nodules, which indicate precipitation from warm (between 32.0 and 48.9 °C) and ^{18}O -enriched fluids ($\delta^{18}\text{O}_{\text{H}_2\text{O}} = 12.3 \pm 1.9\text{‰}$). In addition, all eggshells from QSD Sur have higher $\delta^{13}\text{C}$ values than those from other sites, indicating that they have interacted with ^{13}C -enriched diagenetic fluids. The Δ_{47} -derived temperature (3.3 °C) of the single eggshell analysed from QSD Sur reflects contamination, possibly related to the presence of sulfate, although the Δ_{48} offset and 49 Parameter (Davies and John, 2017) do not show anomalous values (Supplementary data). In contrast, all samples from QSD Norte (eggshells, diagenetic carbonate nodules, sedimentary rock) define separate, tight clusters in their isotopic compositions, with the eggshells having the lowest $\delta^{13}\text{C}$ and highest $\delta^{18}\text{O}$ values, well apart from those of the abiogenic materials. This difference in isotopic compositions also supports a good preservation state, as deduced from optical and chemical methods. Only two samples (LL-108c and LL-108g, see Table 1) have comparatively higher $\delta^{13}\text{C}$ and lower $\delta^{18}\text{O}$ values, similar to the three eggshells from Sanagasta considered as partially preserved (see “outliers” in Fig. 5). It must be noted that a certain degree of spread in the $\delta^{18}\text{O}$ and $\delta^{13}\text{C}$ values for the eggshells collected from the same site is not surprising. In extant birds, some variations are observed between clutches produced by the same colony, and even between the eggs of the same clutch (e.g., barnacle goose *Branta leucopsis*, Pokrovskaya et al., 2011). Such a spread of data is interpreted to be the result of changes in the body fluid composition, caused by water loss (^{18}O -enrichment) during the egg formation, and a

progressive shift (from the diet to the stored fat) of the carbon source used for egg mineralisation (^{13}C -depletion).

In addition, even for the best-preserved eggshells, minor contamination by secondary calcite filling the pores of the eggs (leading to small but non-negligible disturbance in the biogenic $\delta^{13}\text{C}$ and $\delta^{18}\text{O}$ values) cannot be completely avoided when using classical powder sampling methods (i.e., stripping off of the superficial allochthonous material and crushing the central part of the shell). As the pore volume of titanosaurian eggshells can be up to 20% in the eggshells from Sanagasta (see 3D modelling in Hechenleitner et al., 2016a), measuring the stable isotope composition in the matrix of the associated sedimentary rock matrix is crucial to evaluate to which extent secondary carbonates influence the values of biogenic origin, and the direction of the isotope shift. This statement on the sampling method is valid for most studies dealing with titanosaurian eggshells (including the references listed in the next section), with the consequence that even very well-preserved eggshells may have an isotopic composition slightly shifted towards the values of associated carbonate nodules and rocks (higher $\delta^{13}\text{C}$ and lower $\delta^{18}\text{O}$ values). To avoid this issue, high-precision computer-controlled microdrilling might be recommended in future studies.

5.1.2. Low $\delta^{13}\text{C}$ and high $\delta^{18}\text{O}$ values, the hallmark of well-preserved titanosaurian eggshells

Over the last five decades, several studies have reported stable isotope carbon and oxygen isotope compositions of Late Cretaceous

Table 2
Clumped (Δ_{47}) isotope compositions and derived precipitation temperatures for the samples selected in Table 1.

Nesting site	Sample type	Sample ID	Replicates	$\delta^{13}\text{C}_{\text{CO}_3}$	SD	$\delta^{18}\text{O}_{\text{CO}_3}$	SD	$\delta^{18}\text{O}_{\text{CO}_3}$	Δ_{47}	SE	Δ_{47}	SE	Confidence Interval		$\delta^{18}\text{O}_{\text{H}_2\text{O}}^\dagger$	
				‰ VPDB	‰	‰ VPDB	‰	‰ VSMOW	‰	‰	‰	‰	°C	0.68%	0.95%	‰ VSMOW
Sanagasta	Eggshell	LL-119a	19	-8.3	#	-4.2	#	26.5	0.652	###	31.0	2.1	2.1	4.3	-0.67	
		LL-122b	15	-8.6	#	-5.3	#	25.5	0.634	###	37.3	2.9	3.0	6.2	-0.48	
		LL-130b	15	-9.2	0.1	-0.3	#	30.6	0.639	###	36.0	3.2	3.3	6.8	4.22	
	Carbonate nodule	LL-180	8	-7.8	0.1	-5.0	#	25.8	0.647	###	32.8	2.6	2.8	6.1	-1.07	
		Hydrothermal calcite	LL-62	14	-9.1	#	-7.4	0.1	23.3	0.641	###	35.1	2.3	2.4	5.1	-3.01
		LL-175b	9	-9.1	0.1	-6.0	#	24.8	0.645	###	33.2	0.9	0.9	2.0	-1.95	
		LL-100	4	-8.0	0.1	-6.1	#	24.7	0.628	###	39.2	3.0	3.6	9.6	-0.94	
Tama	Carbonate nodule	LL-173c	2	-7.2	#	-5.8	#	24.9	0.628	0.001	39.0	0.8	1.5	10.7	-0.74	
		LL-97	14	-9.5	0.1	-5.8	0.1	25.0	0.637	###	36.4	3.1	3.2	6.8	-1.14	
QSD Sur	Eggshell	LL-105a	15	-5.5	#	-0.7	#	30.2	0.755	###	3.3	1.8	1.8	3.8	-3.05	
	Carbonate nodule	LL-85e	11	-6.7	0.1	7.1	#	38.3	0.643	###	32.0	3.4	3.5	7.5	10.94	
QSD Norte	Eggshell	LL-85 h	4	-6.8	#	6.6	#	37.7	0.600	###	48.9	1.9	2.2	5.9	13.59	
		LL-108b	17	-12.0	0.1	-1.1	#	29.8	0.593	###	52.4	3.8	3.9	8.0	6.44	
	LL-108c	19	-8.6	#	-0.9	0.1	30.0	0.601	###	48.7	2.2	2.3	4.7	5.95		
	LL-108 g	20	-9.8	#	-0.7	0.1	30.2	0.590	###	52.7	1.9	2.0	4.0	6.92		
	LL-82d	19	-12.7	#	1.5	#	32.5	0.622	###	41.3	2.3	2.4	4.9	7.09		
	LL-82f bis	16	-11.8	#	0.4	#	31.3	0.578	###	58.3	3.9	4.0	8.3	8.93		
	Carbonate nodule	LL-81a	10	-9.3	#	-2.6	#	28.2	0.635	0.012	37.4	4.2	4.4	9.5	2.21	
		LL-81 g	18	-8.7	#	-2.3	0.1	28.5	0.617	###	42.9	1.7	1.7	3.5	3.49	

Calculated using the ETH calibration (Bernasconi et al., 2018).

† Calculated using the calcite-water fractionation equation of Kim and O'Neil (1997).

titanosaurian eggshells in mid-palaeolatitudes (23 to 45°, Folinsbee et al., 1970; Erben et al., 1979; Cojan et al., 2003; Kim et al., 2009; Bojar et al., 2010; Riera et al., 2013; Eagle et al., 2015; Dawson et al., 2020). Most $\delta^{13}\text{C}$ and $\delta^{18}\text{O}$ values cluster into three distinct fields (Fig. 6), referred to as Cluster 1, 2 and 3 hereafter.

Folinsbee et al. (1970) focused on titanosaurian ('*Hypselosaurus*') eggshells of Maastrichtian age from Aix-en-Provence (Rousset site), France. The preservation state was considered good with only rare recrystallisation features, and the isotopic compositions they reported ($\delta^{13}\text{C} = -14.5$ to -13.3 ‰ and $\delta^{18}\text{O} = 29.0$ to 30.9 ‰) plot into Cluster 3. Erben et al. (1979), Cojan et al. (2003) and Eagle et al. (2015) also analysed titanosaurian eggshells from the same region. Just as Folinsbee et al. (1970), Erben et al. (1979) also rated the preservation state of the eggshells as good and noted that almost no recrystallisation occurred, while Cojan et al. (2003) and Eagle et al. (2015) were much more cautious with defining a preservation state. Their isotopic compositions plot either into Cluster 2 ($\delta^{13}\text{C} = -10.2$ to -8.4 ‰ and $\delta^{18}\text{O} = 25.2$ to 27.3 ‰, Erben et al., 1979) or spread over Clusters 2 and 3 ($\delta^{13}\text{C} = -15.0$ to -8.0 ‰ and $\delta^{18}\text{O} = 25.0$ to 33.0 ‰, Cojan et al., 2003; $\delta^{13}\text{C} = -13.2$ to -9.2 ‰ and $\delta^{18}\text{O} = 26.0$ to 32.2 ‰, Eagle et al., 2015). The disparate isotopic results reported by the different studies are attributed to the facts that the eggshells were collected in different sites and horizons, had distinct diagenetic histories, and therefore unevenly preserved the original isotopic compositions.

Kim et al. (2009) analysed eggshells with faveoololithid and spheroolithid microstructures from the Gyeongsang Basin, South Korea. Those eggshells were first attributed to herbivorous ornithomimid and sauropod dinosaurs, but some of them (i.e., faveoololithid eggshells) were later attributed to the clade Titanosauria (Fiorelli et al., 2012; Hechenleitner et al., 2015). It is noteworthy that Kim et al. (2009) did not correlate the isotopic compositions they measured with the type of eggs they sampled. The eggshells were regarded originally as well-preserved, although we argue from Fig. 3e in Kim et al. (2009) that they look substantially recrystallised and altered. Most eggshell isotopic

compositions fall within Cluster 2 in Fig. 6 ($\delta^{13}\text{C} = -8.5$ to -8.0 ‰ and $\delta^{18}\text{O} = 25.0$ to 27.5 ‰), and they are well apart from the associated abiogenic carbonates that have extremely low $\delta^{18}\text{O}$ values (down to 8.5‰) compared to those of all the other sites. Some eggshells also have very low $\delta^{18}\text{O}$ values (down to 16‰), i.e., unlike any other titanosaurian eggshells discussed here. We agree with Kim et al. (2009) who hypothesized the contribution of hydrothermal fluids related to the intrusion of the Seonso Fm by magmatic dykes to explain the very low $\delta^{18}\text{O}$ values of those eggshells (see also Choi et al., 2006).

Riera et al. (2013) worked on titanosaurian eggshells of Maastrichtian age from several sites of the southern Pyrenees, Spain. Eggshells showed a good preservation of original microstructures and no evidence for recrystallisation, except in the site of Sallent. The isotopic compositions of the well-preserved eggshells plot into Cluster 3 ($\delta^{13}\text{C} = -15.0$ to -11.3 ‰ and $\delta^{18}\text{O} = 28.0$ to 32.7 ‰), while those from Sallent plot into Cluster 2 ($\delta^{13}\text{C} = -11.3$ to -7.8 ‰ and $\delta^{18}\text{O} = 25.5$ to 29.0 ‰). Sellés et al. (2017) provided additional $\delta^{13}\text{C}$ and $\delta^{18}\text{O}$ values for pathologic specimens from the same sites. They also noticed a very well-preserved microstructure and reported $\delta^{13}\text{C}$ and $\delta^{18}\text{O}$ values similar to those reported by Riera et al. (2013), even though less tightly clustered. Those values show obvious co-variation from Cluster 2 for the atypical – and altered – eggshells from Sallent to Cluster 3 for the best-preserved eggshells. Interestingly, the values of the well-preserved Maastrichtian eggshells from northern Spain analysed by Erben et al. (1979) also plot within Cluster 3 ($\delta^{13}\text{C} = -14.2$ to -11.3 ‰ and $\delta^{18}\text{O} = 30.2$ to 31.6 ‰).

When the preservation state of the titanosaurian eggshell microstructure was unambiguously evaluated as good or excellent, such as in the Maastrichtian samples from the Hațeg Basin, Romania ($\delta^{13}\text{C} = -15.0$ to -12.6 ‰ and $\delta^{18}\text{O} = 29.5$ to 30.8 ‰, Bojar et al., 2010, Grellet-Tinner et al., 2012, Dawson et al., 2020), and in one of the Campanian samples from Auca Mahuevo, Neuquén Province, Argentina ($\delta^{13}\text{C} = -12.7$ ‰ and $\delta^{18}\text{O} = 31.5$ ‰, Eagle et al., 2015), the isotopic compositions invariably plot into Cluster 3. Our results also confirm this view, with the well-preserved eggshells from QSD Norte plotting into Cluster

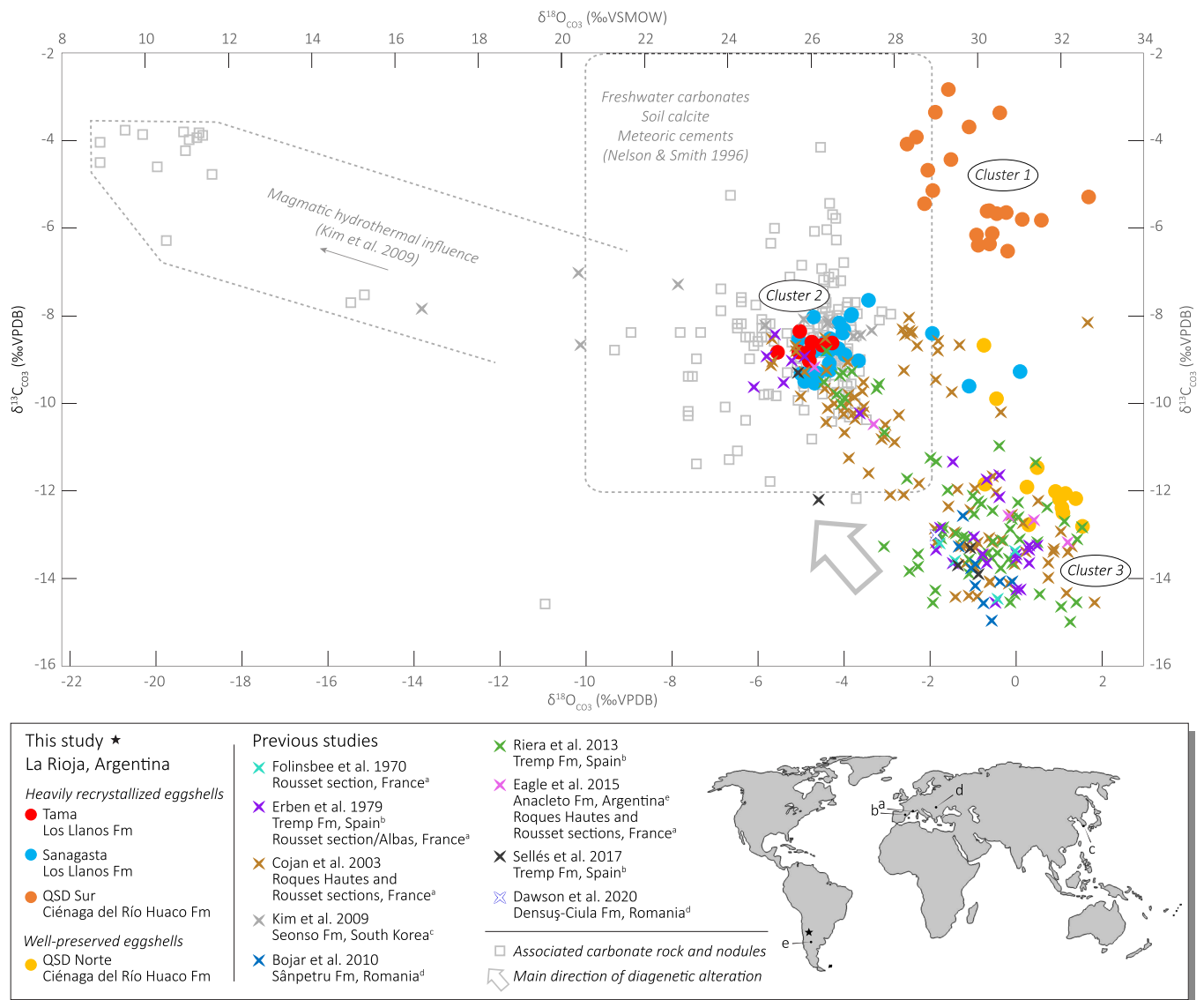


Fig. 6. Carbon and oxygen stable isotope compositions from mid-palaeolatitude (23–45°) titanosaurian eggshells sampled in La Rioja, NW Argentina (star symbol), and in other nesting sites worldwide (see map). Light gray squares represent the associated, abiogenic geological samples published by others. Cluster 1 and 2 contain data from heavily altered eggshells (see text for discussion), while Cluster 3 combines the low $\delta^{13}\text{C}$ and high $\delta^{18}\text{O}$ values characteristic of well-preserved titanosaurian eggshells. QSD = Quebrada de Santo Domingo.

3, and the altered or diagenetic specimens from QSD Sur, respectively from Sanagasta and Tama, into Clusters 1 and 2.

From the above discussion, we conclude that the combination of low $\delta^{13}\text{C}$ (–15 to –11‰) and high $\delta^{18}\text{O}$ (27 to 33‰) values is an excellent indicator of the well-preserved state of Late Cretaceous eggshells produced by mid-palaeolatitude (23° to 45°) titanosaurs. The definition of such an isotopic hallmark for well-preserved eggshells can help to identify cryptic alteration features, and to evaluate the preservation state, e.g., for specimens stored in private collections or museums and for which the associated geological materials are not available. Conversely, the preservation state of the eggshells having isotopic compositions markedly out of this field should be regarded with care, or, in case the preservation state can be proven to be good, point to very specific environmental conditions capable of substantially modifying the isotopic composition of the local carbon and oxygen sources (Kim et al., 2009).

5.1.3. Preservation of isotopic compositions in the titanosaurian tooth

Hard biapatite tissues such as teeth and bones have different

resistance to alteration, mainly because of differences in crystal size, composition and porosity. Large crystal size, low organic matter content and low porosity, favour the preservation of the biogenic stable isotopic compositions in enamel mineralised tissues compared to the more porous, organic matter rich, nanometre-scale crystallinity of tissues such as dentine and bone (e.g., Zazzo et al., 2004). Similar isotopic compositions in different tissues of the same fossil specimen suggest either preservation of original biogenic stable isotope compositions or complete resetting of both tissue types to homogenous values corresponding to the diagenetic conditions. The bioapatite material from a single titanosaurian specimen of QSD Sur has a clear trend in the stable oxygen isotope composition of phosphate, with tooth enamel $\delta^{18}\text{O}_{\text{PO}_4}$ of 18.9‰ being higher than the tooth dentine with $\delta^{18}\text{O}_{\text{PO}_4}$ = 16.9‰ and the associated bone dentine with $\delta^{18}\text{O}_{\text{PO}_4}$ = 16.6‰ (see Table 1). This supports the interpretation that tooth enamel has, at least partially, preserved its original isotopic composition.

The $\delta^{18}\text{O}$ of a given mineral reflects the precipitation temperature and the $\delta^{18}\text{O}$ of the water from which it precipitated (e.g., Kim and O'Neil, 1997). Since phosphate-water and carbonate-water fractionation

factors are different, an offset in the $\delta^{18}\text{O}$ values between tooth hydroxyapatite ($\delta^{18}\text{O}_{\text{PO}_4}$) and structural carbonate ($\delta^{18}\text{O}_{\text{CO}_3}$) is expected in a tooth precipitated from the same body water and at constant body temperature, according to several pieces of evidences supporting sauropod dinosaur homeothermy (endothermy or gigantothermy) (Amiot et al., 2011; Eagle et al., 2011, 2015). In extant homeothermic vertebrates, the $\delta^{18}\text{O}_{\text{CO}_3}$ is 7 to 9‰ higher than the $\delta^{18}\text{O}_{\text{PO}_4}$ (Bryant et al., 1996; Iacumin et al., 1996). In the titanosaurian tooth enamel measured here, this offset is 7.3‰, supporting that both mineral phases are likely to have preserved their original compositions established under conditions of homeothermy.

Finally, the reliability of isotopic data recorded in tooth enamel can also be evaluated based on the correlation proposed by Amiot et al. (2004) between the palaeolatitudinal location L (in degrees) of Late Cretaceous dinosaurs and the $\delta^{18}\text{O}_{\text{PO}_4}$ values obtained from the fossil remains in ‰ (VSMOW):

$$\delta^{18}\text{O}_{\text{PO}_4\text{dinosaurs}} = -0.22L + 26.52 \quad (1)$$

This equation reflects the close relation between the $\delta^{18}\text{O}$ of vertebrate phosphate and that of ingested/meteoric water, which is closely related to the latitude. Although other parameters influence the $\delta^{18}\text{O}_{\text{PO}_4}$ (distance from the shore, altitude, etc.), this equation can be used as an estimate of the bioapatite values expected at our study sites. Considering an approximate palaeolatitude of 32°S for QSD (Hechenleitner et al., 2020), we obtain a $\delta^{18}\text{O}_{\text{PO}_4}$ value of 19.5‰, i.e., very close to the value of 18.9‰ measured in tooth enamel from QSD Sur, and only slightly lower than the values of 20.6‰ and 21.1‰ reported for teeth of other titanosaurs living at similar palaeolatitudes (Trempe Fm, Spain, Domingo et al., 2015).

In summary, the difference in $\delta^{18}\text{O}$ values between enamel, dentine and bone, as well as the offset in isotopic compositions between tooth phosphate and structural carbonate, and the similarities between calculated and estimated paleolatitudes (and with those published by others), together with the dark blue CL colour and the low REE content reported from analytical techniques (see Figs. 3 and 4), we conclude that the data measured in tooth enamel from QSD Sur reliably reflect the original biogenic compositions and are well-suited for further interpretation.

5.2. Thermoregulation, diet, and reproduction of titanosaurs

5.2.1. Constant, elevated body temperature

The body temperature of titanosaurs during the egg-laying period can be calculated from the Δ_{47} values measured in well-preserved eggshells, since these record the body temperature of the mother. However, well-preserved bulk isotopic compositions ($\delta^{13}\text{C}$ and $\delta^{18}\text{O}$) do not guarantee the preservation of the original Δ_{47} values. In QSD Norte eggs indeed, most Δ_{47} -derived temperatures are too high (up to 58 °C) and physiologically unrealistic. Alteration of the Δ_{47} can occur in a closed system through thermally induced solid-state C—O bonds reordering (e.g., Stolper and Eiler, 2015). Such internal isotope-exchange reactions are thought to take place when the carbonate is exposed to temperatures greater than 80–100 °C during millions of years (Henkes et al., 2014; Stolper and Eiler, 2015). Given that the Andean orogeny was already an ongoing process during the Late Cretaceous (Martínez et al., 2017), and considering the regional geology of Quebrada de Santo Domingo where the Cenozoic cover does not exceed 1000 m in thickness (Limarino et al., 2016), the maximal burial depth of the eggs was probably not sufficient for such temperatures to be reached. However, if egg calcite is less resistant to clumped isotope reordering than the calcites experimentally tested by Henkes et al. (2014) and Stolper and Eiler (2015), they could have experienced partial reordering at even lower temperatures. This could also be responsible for the observed range in temperatures between 41.3 and 58.3 °C for QSD Norte eggs (Table 2). Unexpectedly low Δ_{47} values could reflect a larger proportion of secondary carbonate (that

would have formed at higher temperature) in some parts of the eggshell. In that case however, we would also expect a difference in the bulk isotopic composition of the replicates that yielded the lowest Δ_{47} values (and highest derived temperatures), which again was not observed in our data.

Interestingly, the eggshell specimen from QSD Norte with the lowest $\delta^{13}\text{C}$ and highest $\delta^{18}\text{O}$ values (LL-82d; i.e., presumably the best-preserved eggshell specimen of all according to the isotopic hallmark we defined in Section 5.1.2.) also has the lowest body temperature, with 41.3 ± 4.9 °C (calculated from 19 replicates). This sample also has the most distinct bulk isotopic composition, which clearly stands out compared to the abiogenic associated carbonate (see Fig. 6), and suggests that the participation of secondary carbonate is the lowest of all our egg samples. We consider this sample to be the closest to the real titanosaurian body temperature, in reasonable agreement with the average body temperature of 37.6 ± 1.9 °C calculated by Eagle et al. (2015) when the error is considered. It must be noted that those authors have reported a wide spread of data, with temperatures higher than 41 °C for two-thirds of the eggshells cited as “apparently well-preserved” (Auca Mahuevo, Level 4) and used to calculate the average body temperature of 37.6 °C. According to Amiot et al. (2006), a body temperature over 39 °C is lethal for extant low latitude reptiles, but other terrestrial vertebrates like extant birds can have a body temperature over 40 °C (as high as 44.6 °C for the sombre hummingbird *Aphantochroa cirrochloris*, Eagle et al., 2015, and up to 45 °C for the desert bird Burchell's sandgrouse *Pterocles burchelli* under laboratory conditions, McKechnie et al., 2016). Although a comparison between small birds and titanosaurs of a radically different size is limited since the metabolic rate responds to body mass (e.g., White and Seymour, 2003; Ganse et al., 2011), it is worth opening the question as to whether titanosaurian body temperature could have been close to or even slightly above 40 °C.

The thermoregulation strategy adopted by titanosaurs and other sauropods (i.e., whether they were homeo- or poikilothermic), has long been debated. However, an increasing number of studies supports the scenario of a constant body temperature (homeothermy) for several dinosaur taxa. Clues about thermoregulation can be obtained from tooth enamel and the different fractionation factors between carbonates, respectively phosphates, and water. In extant homeothermic vertebrates, the offset between dental $\delta^{18}\text{O}_{\text{CO}_3}$ and $\delta^{18}\text{O}_{\text{PO}_4}$ values is on the order of 7 to 9‰ (Bryant et al., 1996; Iacumin et al., 1996). In the tooth enamel sample analysed here, this offset is within this range at 7.3‰, suggesting that dental development in titanosaurs occurred under constant temperature, well in line with the recent articles on sauropod dinosaur homeothermy (Amiot et al., 2006; Eagle et al., 2011, 2015). Finally, the isotopic hallmark defined in Section 5.1.2. for mid-palaeolatitude titanosaurian eggshells reflects a relatively narrow $\delta^{18}\text{O}$ range (Cluster 3), further supporting their formation at a relatively constant body temperature (homeothermy).

5.2.2. Plants with C3 metabolic pathway as staple food

The $\delta^{13}\text{C}$ values of terrestrial herbivorous vertebrates is linked to their diet and mainly reflects whether they were ingesting C3 plants, C4 plants, or a mix of both. The isotopic differences between these two kinds of plants result from distinct photosynthetic pathways (Farquhar et al., 1989). The $\delta^{13}\text{C}$ values of extant C3 plants range between -37 and -20 ‰ (Farquhar et al., 1989) with an average value of -28 ‰ (Kohn, 2010), while those of C4 plants are between -16 and -12 ‰ (O'Leary, 1981). For the Late Cretaceous, the general consensus is that only C3 plants were available for terrestrial herbivores (Osborne and Beerling, 2006; Kohn, 2010), while the presence of Cretaceous C4 plants is limited to a single isotopic record so far (Kuypers et al., 1999). The difference between the $\delta^{13}\text{C}$ value of plants and that of the source carbon (i.e., atmospheric CO_2) depends on the carbon isotope discrimination occurring during photosynthesis. This discrimination varies along with a combination of environmental and species-specific physiological

factors, e.g., the partial pressure of atmospheric CO₂, the water supply or the stomatal conductance of the leaves (Cernusak et al., 2013). Other environmental parameters such as the altitude and the latitude further influence the carbon isotope composition of plants (Kohn, 2010) and the initial δ¹³C value of the past atmospheric CO₂ is of course also crucial. The best δ¹³C estimates for the Campanian-Maastrichtian atmospheric CO₂ are around -6‰, vs. -8 to -7‰ for present values (Coplen et al., 2002; Barral et al., 2017). This suggests that Late Cretaceous C3 plants possibly had an isotopic range shifted towards higher values compared to the present range.

Carbon assimilation by living organisms and its subsequent fixation in biomineralised tissues, including eggshells and teeth, occur through physiological reactions that induce isotopic fractionation. Several ¹³C-enrichment factors between diet and mineralised tissues (oological calcite or tooth structural carbonate) are published for extant avian dinosaurs: 14 to 16‰ for unspecified birds (Koch, 2007), 15 to 16‰ for ratites (Ségalen and Lee-Thorp, 2009), 13 to 16‰ for herbivorous birds (Hobson, 1995; Johnson et al., 1998; Cojan et al., 2003; Bojar et al., 2010; Angst et al., 2014), 8‰ for carnivorous birds (Angst et al., 2014), and 16‰ for large birds (Johnson et al., 1998). Among extinct dinosaurs, Fricke et al. (2008) reported 18‰ of ¹³C-enrichment between bioapatite structural carbonate of hadrosaurs and their diet, while Tütken (2011) estimated a 16‰ enrichment for sauropods. Thus, ¹³C-enrichment factors in the order of 13 to 18‰ are widely accepted between oological calcite in most birds, respectively tooth structural carbonate in large herbivorous dinosaurs, and their diet. Subtracting those factors from the average δ¹³C values of -11.7‰ measured in the well-preserved eggshells from QSD Norte, we obtain δ¹³C values of -29.7 to -24.7‰ for their plant diet. These strongly support the view that plants with a C3 metabolic pathway were the staple diet of Late Cretaceous titanosaurs.

Plants under high water stress tend to show a weaker carbon isotope discrimination from the atmospheric CO₂ and thus have higher δ¹³C values (Kohn, 2010; Cernusak et al., 2013; Barral et al., 2017), and models have been developed to calculate the mean annual precipitation based on plant values (e.g., Kohn, 2010). However, the relatively wide range estimated for QSD plant δ¹³C values – which reflects the uncertainties regarding the ¹³C-enrichment factor between plants and titanosaurian egg calcite – hinders reliable estimates of the amount of precipitation. Nevertheless, according to Kohn's (2010) model (which corrects for palaeolatitude, altitude, atmospheric δ¹³C and physiological fractionation), a ¹³C-enrichment of 18‰ between plant and egg calcite results in unrealistic precipitation rates (between 5300 and 6700 mm/year, even when considering a wide range of palaeoaltitudes, i.e., 100 to 3000 m.a.s.l.). An enrichment factor of 16‰ results in precipitation rates that are excessively high (>2000 mm/year) in our palaeoenvironmental context. This suggests that the ¹³C-enrichment factor between plants and titanosaurian egg calcite was probably lower than 16‰.

5.2.3. Hydrothermalism and titanosaurian reproduction

The role of hydrothermalism in titanosaurian egg incubation at Sanagasta can be evaluated from hydrothermal crystals provided that both occurrences were contemporaneous, as previously suggested for this site (Grellet-Tinner and Fiorelli, 2010). Water in continental hydrothermal systems has either a meteoric (resulting from atmospheric precipitation) or a magmatic (released by a magmatic system) origin, or a mix of both (common in geothermal systems). Meteoric water typically represents surface runoff (creeks, rivers), infiltrated vadose zone or finally groundwater that may become sufficiently heated at larger depths of infiltration such as in geothermal systems, before upwelling to the surface through thermal convection (Renner et al., 1975). In contrast, magmatic water originates from the release of fluids by crystallising magmatic bodies (e.g., Hedenquist and Lowenstern, 1994). Because of their very specific origins and fractionation processes, meteoric and magmatic water can be confidently discriminated via the stable oxygen and/or hydrogen isotopic compositions of the minerals

formed by hydrothermal activity.

The average δ¹⁸O values measured in hydrothermal calcite and quartz from Sanagasta are 25.0 and 32.0‰, respectively (Fig. 5). In contrast, the δ¹⁸O values of the silicate clasts eroded from the surrounding Carboniferous Sanagasta granite average 11.9‰, which clearly points to a magmatic origin (plutonic rocks usually have δ¹⁸O values between 5 and 15‰; Sheppard, 1986; Hoefs, 2009), possibly with some degree of crustal contamination (Macchioli Grande et al., 2020). The average Δ₄₇-derived temperature for hydrothermal calcite precipitation is 37 °C (33 to 39 °C) and the average δ¹⁸O_{H2O} value for the water is -1.7‰ (-3.0 to -0.7‰) using the equation of Kim and O'Neil (1997). While this value is relatively high for purely surface-derived meteoric water, it is not uncommon in arid continental environments. In addition, the enrichment in ¹⁸O may be related to hydrothermal fluid-rock interaction with the underlying basement, if the meteoric waters were heated to close to 100 °C (McKibbin et al., 1986; Criss et al., 1991; Rollinson, 1993). The validity of this result can be cross-checked using the quartz-water oxygen isotope fractionation. Using the equation of Sharp et al. (2016) with a δ¹⁸O_{H2O} value of -1.7‰ calculated for the hydrothermal calcite and the δ¹⁸O_{SiO2} of hydrothermal quartz (see Table 1), we obtain an average precipitation temperature of 37.1 °C (29.9 to 43.1 °C), consistent with the Δ₄₇-based temperature of the hydrothermal calcite. The close cross-matching between those results supports the idea that hydrothermal calcite and quartz precipitated at a low temperature ranging between roughly 30 and 43 °C, and that the δ¹⁸O_{H2O} values likely represent exchanged meteoric water or, alternatively, unexchanged meteoric waters typical for arid continental regions and where the range of water values may well reflect the seasonal variation typical for meteoric precipitation. In addition, the coexistence of hydrothermal calcite and quartz indicates that the Sanagasta hydrothermal fluids had dynamic pH values, as both minerals require different pH conditions to precipitate. This is commonly explained by alternate precipitation, in which the formation of one mineral species is accompanied by a change in pH beneficial to the growth of the other (e.g., Bustillo, 2010). The low thermal water temperatures calculated here are similar to incubation temperatures measured in extant ostriches (33 to 37 °C, Cooper, 2001) and megapodes (30 to 38 °C, Göth, 2007), or calculated for extinct dinosaurs (35 to 40 °C in oviraptorids, Amiot et al., 2017). This suggests that the hydrothermal activity in Sanagasta could have been used as a heat source by titanosaurs for egg incubation, as previously proposed by others (Grellet-Tinner and Fiorelli, 2010; Fiorelli et al., 2012).

5.2.4. Ideal conditions for titanosaurian nesting

The level of aridity prevailing during the reproduction of titanosaurs can be estimated based on the oxygen isotopic values of their eggshells, as they reflect the meteoric (i.e., ingested) water at the time of their formation. The oxygen isotopic composition of titanosaurian body water (δ¹⁸O_{H2O}) can be calculated via the calcite-water fractionation equation (Kim and O'Neil, 1997), using the Δ₄₇-derived body temperature. However, although the best-preserved eggshells of QSD Norte show close to pristine bulk isotopic compositions, their Δ₄₇ values probably do not reflect the real body temperature. Using a hypothetical titanosaurian body temperature of 37 °C, in agreement with previously published Δ₄₇-derived temperatures for this taxon (Eagle et al., 2015; Dawson et al., 2020), we calculate a body water δ¹⁸O of +5.3‰. As a comparison, Eagle et al. (2015) obtained a similar δ¹⁸O_{H2O} value of 5.2‰ for Auca Mahuevo titanosaurian eggs using Δ₄₇-derived temperatures. Since the physiological reactions involved in the ingestion and assimilation of meteoric water favour the heavy oxygen isotope, body water is typically enriched in ¹⁸O with respect to meteoric water, between 4 and 8‰ in extant terrestrial birds (Lazzerini et al., 2016). Assuming that similar enrichment processes occurred for titanosaurs, we obtain after subtraction a δ¹⁸O_{H2O} of -2.7 to 1.3‰ for meteoric water at Quebrada de Santo Domingo.

Using the titanosaurian tooth enamel δ¹⁸O_{PO4} (18.9‰) and the

water-phosphate fractionation equation by Lécuyer et al. (2013) a much lower $\delta^{18}\text{O}_{\text{H}_2\text{O}}$ value of 1.0‰ for the titanosaurian body water is obtained, while the calculated meteoric water becomes -7.0 to -3.0 ‰ (see Table 1) after subtraction of the ^{18}O -enrichment factors of Lazzzerini et al. (2016) (Fig. 7). This suggests a difference in the evaporation conditions between the period of tooth formation (average of several weeks to months) and eggshell formation (days to week).

To reliably interpret the 4‰ difference between the $\delta^{18}\text{O}_{\text{H}_2\text{O}}$ values of body (and meteoric water values) derived from the eggshells (5.3‰, respectively -2.7 to 1.3‰) and from the tooth enamel (1.0‰, respectively -7.0 to -3.0 ‰), the rate at which each of these tissues biomineralises and records the ambient water $\delta^{18}\text{O}$ values must be evaluated. As eggshells form within days or weeks, their $\delta^{18}\text{O}_{\text{CO}_3}$ values reflect the isotopic composition of body and meteoric water during the reproduction period, and, in particular, during the eggshell formation. It has been shown that the turnover of oxygen and carbon isotopes in the body water of mammals and birds occurs within days, meaning that changes in diet and ingested water quickly impact the stable isotope composition of rapidly growing biomineralised tissues such as eggshells (Hobson, 1995; Podlesak et al., 2008). In contrast, sauropod teeth form over weeks to months (D'Emic et al., 2013), and their $\delta^{18}\text{O}$ values reflect a long-term average of the body and meteoric water. The $\delta^{18}\text{O}$ values obtained in the samples from the Quebrada de Santo Domingo material suggest that reproduction and oviposition in titanosaurians occurred under conditions more arid than the long-term average. This observation is consistent with the floodplain facies in which the eggs are preserved, which would have made a very inhospitable nesting ground during the wet season, considering the risk of flooding. The $\delta^{18}\text{O}$ values derived from tooth enamel suggest either an alternation of wet and dry climatic conditions, or migration of titanosaurians towards more arid areas during the nesting period (or a combination of both).

Although we cannot definitively exclude at this stage that Quebrada de Santo Domingo could have been used as a permanent living ground, several indicators suggest that this site was preferred for nesting and that titanosaurians periodically returned to lay their eggs (reproductive philopatry). This site represented an ideal nesting site for titanosaurians, since it has been repetitively used over several reproductive episodes, as suggested by the massive amount of eggs preserved in several

stratigraphic levels. The large quantity of eggs in close association also points to a gregarious behaviour of titanosaurians, or at least among the females during the nesting period. A herd behaviour linked to reproduction brings into perspective other aspects of titanosaurian physiology and habitat. Several studies have explored the nutritional value of a sauropod diet and the amount of plant matter that a large sauropod dinosaur should ingest in order to get sufficient energy (e.g., Hummel and Clauss, 2011; Sander et al., 2011; Gill et al., 2018), especially if they maintained an elevated, constant body temperature. The large resource requirement exerted on the vegetation by a herd of large titanosaurians favours the hypothesis of a migratory behaviour over sedentariness, and further supports the idea that titanosaurians were philopatric animals. However, we cannot rule out the possibility that titanosaurians experienced periods of fasting during reproduction, or, more specifically, oviposition. Periodic fasting in extant animals is common and occurs when feeding becomes of lesser importance compared to other needs, such as moulting or, precisely, reproduction (Castellini and Rea, 1992; Groscolas and Robin, 2001; McCue, 2013). By analogy to extant organisms, titanosaurians from Quebrada de Santo Domingo would have been well set to endure fasting, starting with a good fasting endurance due to their large size and the proportionally high amount of stored fat (Lindstedt and Boyce, 1985; Groscolas and Robin, 2001). Furthermore, since it is unlikely that titanosaurians provided parental care (considering the striking difference in size between adults and offspring, e.g., Sander et al., 2011), breeding activities were limited to mating, egg production and laying, which would considerably narrow down the duration of hypothetical fasting. Also, larger homeothermic animals have a broader range of thermal neutrality (Lindstedt and Boyce, 1985; Chérel et al., 1988), implying that the energy normally used for thermoregulation would become negligible if fasting occurred when ambient temperatures were close to body temperature. Under this perspective, reproduction-related fasting would have been energetically more effective if titanosaurian egg production and oviposition occurred under warm (seasonally and/or geographically driven) conditions.

6. Conclusion

Based on an extensive isotopic database compiled from this and other

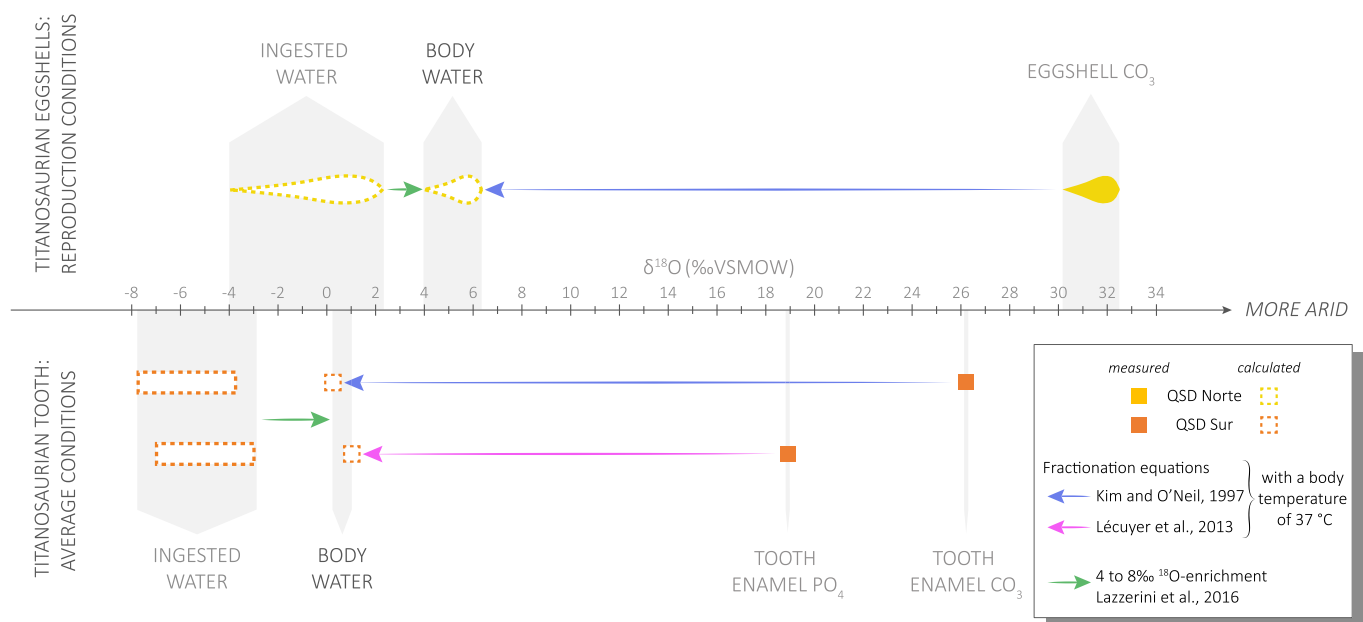


Fig. 7. Oxygen isotopic composition ($\delta^{18}\text{O}$) of body and ingested water calculated from that of the eggshells (upper half), and the tooth (lower half), using a body temperature estimate based on literature data (Eagle et al., 2015; Dawson et al., 2020). Higher $\delta^{18}\text{O}$ values are observed for body water when calculations are made from the eggshells than the tooth, suggesting more arid conditions during the reproduction period. QSD = Quebrada de Santo Domingo.

studies, an isotopic hallmark ($\delta^{13}\text{C}_{\text{VPDB}} = -15$ to -11‰ ; $\delta^{18}\text{O}_{\text{VSMOW}} = 27$ to 33‰) has been proposed to identify the well-preserved eggshells produced by mid-palaeolatitude (23° to 45°) titanosaurs. This hallmark may serve as a geochemical reference to select eggshell samples best suited for reconstructing the palaeoenvironment in which titanosaurs used to reproduce, especially when the alteration is cryptic or when associated abiogenic material such as rocks or nodules are not available for comparative studies. Eggshells with compositions out of this range should be interpreted with care regarding their preservation state, but could potentially reflect peculiar environmental conditions (e.g., volcanic influence).

Stable isotope compositions of biogenic and abiogenic samples from the nesting sites of Sanagasta, Tama and Quebrada de Santo Domingo, NW Argentina, support that titanosaurs were likely homeothermic sauropods with elevated body temperature, at least for the females. Given the high amount of energy required to maintain an elevated body temperature, and therefore, the large demands exerted on food resources (plants having C3 metabolic pathways), titanosaurs likely had a nomadic lifestyle, with population movements driven by seasonality, food availability, and reproductive cycles. These observations, in addition to the high concentration of eggs in specific nesting localities support the idea that titanosaurs were philopatric. The present data also suggest that reproduction occurred under relatively arid environmental conditions. This aridity may either reflect climatic seasonality or migration, or a combination of both, interpretations that are also compatible with our estimates of the oxygen isotope compositions of meteoric waters. By analogy to extant vertebrates, titanosaurs could have experienced reproduction-related fasting, in which case high ambient temperatures would have been energetically more favourable, limiting the costs of thermoregulation. Finally, our study supports that titanosaurs could take advantage of hydrothermal heat for egg incubation.

Declaration of Competing Interest

The authors declare that they have no known competing financial interests or personal relationships that could have appeared to influence the work reported in this paper

Acknowledgements

Many thanks to Dr. Benita Putlitz for measuring the oxygen stable isotope compositions of the silicate samples. Many thanks to Madalina Jaggi and Stewart Bishop for their work and support at the ETH lab, and to Sergio de la Vega and Tonino Bustamante from CRILAR. Thank you to the Secretaría de Cultura de La Rioja, Municipalidad de Sanagasta and Tama, and Gobierno de La Rioja, to the Grupo Roggio and all Quebrada de Santo Domingo supports and funds. This work was supported by the Jurassic Foundation (grant to L.L. and E.M.H., 2016), the Paleontological Society (PalSIRP Sepkoski grants to L.L., L.E.F. and E.M.H., 2015, 2017), the Agencia Nacional de Promoción Científica y Tecnológica (ANPCyT2012-0421 and ANPCyT 2018-01211 to L.E.F.), and the Proyecto Sanagasta-Tama 2007–2010 (Gobierno de La Rioja) to L.E.F. Finally, thank you to Dr. Christophe Lécuyer and two anonymous reviewers for their comments and suggestions.

Appendix A. Supplementary data

Supplementary data to this article can be found online at <https://doi.org/10.1016/j.chemgeo.2021.120452>.

References

- Amiot, R., Lécuyer, C., Buffetaut, É., Fluteau, F., Legendre, S., Martineau, F., 2004. Latitudinal temperature gradient during the Cretaceous Upper Campanian-Middle Maastrichtian: $\delta^{18}\text{O}$ record of continental vertebrates. *Earth Planet. Sci. Lett.* 226, 255–272.

- Amiot, R., Lécuyer, C., Buffetaut, É., Escarguel, G., Fluteau, F., Martineau, F., 2006. Oxygen isotopes from biogenic apatites suggest widespread endothermy in Cretaceous dinosaurs. *Earth Planet. Sci. Lett.* 246, 41–54.
- Amiot, R., Wang, X., Zhou, Z., Wang, X., Buffetaut, É., Lécuyer, C., Ding, Z., Fluteau, F., Hibino, T., Kusuhashi, N., Mo, J., Suteethorn, V., Wang, Y., Xu, X., Zhang, F., 2011. Oxygen isotopes of East Asian dinosaurs reveal exceptionally cold Early Cretaceous climates. *Proc. Natl. Acad. Sci. U. S. A.* 108, 5179–5183.
- Amiot, R., Wang, X., Wang, S., Lécuyer, C., Mazin, J.-M., Mo, J., Flandrois, J.-P., Fourel, F., Wang, X., Xu, X., Zhang, Z., Zhou, Z., 2017. $\delta^{18}\text{O}$ -derived incubation temperatures of oviraptorosaur eggs. *Palaeontology* 1–15.
- Angst, D., Lécuyer, C., Amiot, R., Buffetaut, É., Fourel, F., Martineau, F., Legendre, S., Abourachid, A., Herrel, A., 2014. Isotopic and anatomical evidence of an herbivorous diet in the Early Tertiary giant bird *Gastornis*. Implications for the structure of Paleocene terrestrial ecosystems. *Naturwissenschaften* 101, 313–322.
- Araújo, R., Castaninha, R., Martins, R.M.S., Mateus, O., Hendrickx, C., Beckmann, F., Schell, N., Alves, L.C., 2013. Filling the gaps of dinosaur eggshell phylogeny: Late Jurassic Theropod clutch with embryos from Portugal. *Sci. Rep.* 3, 1924.
- Barral, A., Gomez, B., Legendre, S., Lécuyer, C., 2017. Evolution of the carbon isotope composition of atmospheric CO_2 throughout the Cretaceous. *Palaeogeogr. Palaeoclimatol. Palaeoecol.* 471, 40–47.
- Basilici, G., Hechenleitner, E.M., Fiorelli, L.E., Führ, P., Bó, D., Philip, N., 2017. Preservation of titanosaur egg clutches in Upper Cretaceous cumulative palaeosols (Los Llanos Formation, La Rioja, Argentina). *Palaeogeogr. Palaeoclimatol. Palaeoecol.* 482, 83–102.
- Baumgartner-Mora, C., Baumgartner, P.O., 1994. Shell structure of fossil foraminifera studied by cathodoluminescence. *Microsc. Anal.* 3, 35–38.
- Bernasconi, S.M., Hu, B., Wacker, U., Fiebig, J., Breitenbach, S.F.M., Rutz, T., 2013. Background effects on Faraday collectors in gas-source mass spectrometry and implications for clumped isotope measurements. *Rapid Commun. Mass Spectrom.* 27, 603–612.
- Bernasconi, S.M., Müller, I.A., Bergmann, K.D., Breitenbach, S.F.M., Fernandez, A., Hodell, D.A., Jaggi, M., Meckler, A.N., Millan, I., Ziegler, M., 2018. Reducing uncertainties in carbonate clumped isotope analysis through consistent carbonate-based standardization. *Geochem. Geophys. Geosyst.* 1–20.
- Bojar, A.V., Csiki, Z., Grigorescu, D., 2010. Stable isotope distribution in Maastrichtian vertebrates and paleosols from the Hateg Basin, South Carpathians. *Palaeogeogr. Palaeoclimatol. Palaeoecol.* 293, 329–342.
- Bravo, A.M., Buscalioni, Á.D., Merino, L., Müller, B.G., 2003. Experimental taphonomy of avian eggs and eggshells: effects on early diagenesis. *Palaeovertebrata* 32, 77–95.
- Bryant, D.J., Koch, P.L., Froelich, P.N., Showers, W.J., Genna, B.J., 1996. Oxygen isotope partitioning between phosphate and carbonate in mammalian apatite. *Geochim. Cosmochim. Acta* 60, 5145–5148.
- Burman, J., Gustafsson, O., Segl, M., Schmitz, B., 2005. A simplified method of preparing phosphoric acid for stable isotope analyses of carbonates. *Rapid Commun. Mass Spectrom.* 19, 3086–3088.
- Bustillo, M.A., Alonso-Zarza, A., Tanner, L.H., 2010. Silicification of continental carbonates. In: *Carbonates in Continental Settings: Processes, Facies and Applications*. Developments in Sedimentology Series, Vol. 62. Elsevier, Oxford, pp. 153–174.
- Carignano, A.P., Hechenleitner, E.M., Fiorelli, L.E., 2013. Hallazgo de ostrácodos (Crustacea) Cretácicos continentales en la formación Los Llanos, localidad de Tama, La Rioja. *Ameghiniana* 50, R39.
- Castellini, M.A., Rea, L.D., 1992. The biochemistry of natural fasting at its limits. *Experientia* 48, 575–582.
- Cerling, T.E., Harris, J.M., 1999. Carbon isotope fractionation between diet and biapatite in ungulate mammals and implications for ecological and paleoecological studies. *Oecologia* 120, 347–363.
- Cernusak, L.A., Ubierna, N., Winter, K., Holtum, J.A.M., Marshall, J.D., Farquhar, G.D., 2013. Tansley review Environmental and physiological determinants of carbon isotope discrimination in terrestrial plants. *New Phytol.* 200, 950–965.
- Cherel, Y., Robin, J.P., Walch, O., Karmann, H., Netchitailo, P., Le Maho, Y., 1988. Fasting in king penguin. I. Hormonal and metabolic changes during breeding. *Am. J. Physiol. Regul. Integr. Comp. Physiol.* 254.
- Chiappe, L.M., Coria, R., Dingus, L., Jackson, F., Chinsamy, A., Fox, M., 1998. Sauropod dinosaur embryos from the Late Cretaceous of Patagonia. *Nature* 396, 258–261.
- Chiappe, L.M., Coria, R.A., Jackson, F., Dingus, L., 2003. The Late Cretaceous nesting site of Auca Mahuevo (Patagonia, Argentina): eggs, nests, and embryos of titanosaurian sauropods. *Palaeovertebrata* 32, 97–108.
- Choi, S.-G., Pak, S.J., Kim, C.S., Ryu, I.-C., Wee, S.-M., 2006. The origin and evolution of mineralizing fluids in the Cretaceous Gyeongsang Basin, Southeastern Korea. *J. Geochem. Explor.* 89, 61–64.
- Ciccioli, P.L., Ballent, S., Tedesco, A.M., Barreda, V., Limarino, C.O., 2005. Hallazgo de depósitos cretácicos en la Precordillera de La Rioja (Formación Ciénaga del Río Huaco). *Rev. Asoc. Geol. Argent.* 60, 122–131.
- Clark, I.D., Fritz, P., 1997. *Environmental Isotopes in Hydrogeology*. Lewis Publishers, New York (328 pp.).
- Cojan, I., Renard, M., Emmanuel, L., 2003. Palaeoenvironmental reconstruction of dinosaur nesting sites based on a geochemical approach to eggshells and associated palaeosols (Maastrichtian, Provence Basin, France). *Palaeogeogr. Palaeoclimatol. Palaeoecol.* 191, 111–138.
- Cooper, R.G., 2001. Handling, incubation, and hatchability of ostrich (*Struthio camelus* var. domesticus) eggs: a review. *Poultry Sci. Assoc.* 10, 262–273.
- Coplen, T.B., Hopple, J.A., Böhlke, J.K., Peiser, H.S., Rieder, S.E., Krouse, H.R., Rosman, K.J.R., Vocke, R.D., Révész, K.M., Lambert, A., Taylor, P., de Bièvre, P., 2002. Compilation of minimum and maximum isotope ratios of selected elements in

- naturally occurring terrestrial materials and reagents. In: Water-Resources Investigations Report 01-4222, U.S. Geological Survey (98 pp.).
- Criss, R.E., Fleck, R.J., Taylor, H.P., 1991. Tertiary meteoric hydrothermal systems and their relation to ore deposition, Northwestern United States and Southern British Columbia. *J. Geophys. Res.* 96, 13335–13356.
- Davies, A.J., John, C.M., 2017. Reducing contamination parameters for clumped isotope analysis: the effect of lowering PorapakTM Q trap temperature to below -50°C . *Rapid Commun. Mass Spectrom.* 31, 1313–1323.
- Dawson, R.R., Field, D.J., Hull, P.M., Zelenitsky, D.K., Therrien, F., Affek, H.P., 2020. Eggshell geochemistry reveals ancestral metabolic thermoregulation in Dinosauria. *Sci. Adv.* 6, 1–10.
- D'Emic, M.D., Whitlock, J.A., Smith, K.M., Fisher, D.C., Wilson, J.A., 2013. Evolution of high tooth replacement rates in sauropod dinosaurs. *PLoS One* 8, 1–7.
- DeNiro, M.J., Epstein, S., 1976. You are what you eat (plus a few permil): the carbon isotope cycle in food chains. *Geol. Soc. Am. Abstr. Programs* 8, 834–835.
- DeNiro, M.J., Epstein, S., 1978. Influence of diet on the distribution of carbon isotopes in animals. *Geochim. Cosmochim. Acta* 42, 495–506.
- Dennis, K.J., Affek, H.P., Passey, B.H., Schrag, D.P., Eiler, J.M., 2011. Defining an absolute reference frame for 'clumped' isotope studies of CO_2 . *Geochim. Cosmochim. Acta* 75, 7117–7131.
- Domingo, L., Barroso-Barcenilla, F., Cambra-Moo, O., 2015. Seasonality and paleoecology of the Late Cretaceous multi-taxa vertebrate assemblage of 'Lo Hueco' (central eastern Spain). *PLoS One* 10, 1–25.
- Eagle, R.A., Tütken, T., Martin, T.S., Tripathi, A.K., Fricke, H.C., Connely, M., Cifelli, R.L., Eiler, J.M., 2011. Dinosaur body temperatures determined from isotopic (^{13}C - ^{18}O) ordering in fossil biominerals. *Science* 333, 443–445.
- Eagle, R.A., Enriquez, M., Grellet-Tinner, G., Pérez-Huerta, A., Hu, D., Tütken, T., Montanari, S., Loyd, S.J., Ramirez, P., Tripathi, A.K., Kohn, M.J., Cerling, T.E., Chiappe, L.M., Eiler, J.M., 2015. Isotopic ordering in eggshells reflects body temperatures and suggests differing thermophysiology in two Cretaceous dinosaurs. *Nat. Commun.* 6, 8296.
- Erben, H.K., Hoefs, J., Wedepohl, K.H., 1979. Paleobiological and isotopic studies of eggshells from a declining dinosaur species. *Paleobiology* 5, 380–414.
- Ezpeleta, M., Dávila, F.M., Astini, R.A., 2006. Estratigrafía y paleoambientes de la Formación Los Llanos (La Rioja): una secuencia condensada miocena en el antepaís fragmentado andino central. *Rev. Asoc. Geol. Argent.* 61, 171–186.
- Fadel, A., Zigaite, Z., Blom, H., Pérez-Huerta, A., Jeffries, T., Märss, T., Ahlberg, P.E., 2015. Palaeoenvironmental signatures revealed from rare earth element (REE) compositions of vertebrate microremains of the Vesiku Bone Bed (Homerian, Wenlock), Saaremaa Island, Estonia. *Estonian J. Earth Sci.* 64, 36–41.
- Farquhar, G.D., Ehleringer, J.R., Hubick, K.T., 1989. Carbon isotope discrimination and photosynthesis. *Annu. Rev. Plant Physiol. Plant Mol. Biol.* 40, 503–537.
- Fiorelli, L.E., Grellet-Tinner, G., Alasino, P.H., Argañaraz, E., 2012. The geology and paleoecology of the newly discovered Cretaceous neosauropod hydrothermal nesting site in Sanagasta (Los Llanos Formation), La Rioja, Northwest Argentina. *Cretac. Res.* 35, 94–117.
- Fiorelli, L.E., Leardi, J.M., Hechenleitner, E.M., Pol, D., Basilić, G., Grellet-Tinner, G., 2016. A new Late Cretaceous crocodyliform from the western margin of Gondwana (La Rioja Province, Argentina). *Cretac. Res.* 60, 194–209.
- Folinsbee, R.E., Fritz, P., Krouse, H.R., Robblee, A.R., 1970. Carbon-13 and oxygen-18 in dinosaur, crocodile, and bird eggshells indicate environmental conditions. *Science* 168, 1353–1355.
- Fricke, H.C., Rogers, R.R., Backlund, R., Dwyer, C.N., Echt, S., 2008. Preservation of primary stable isotope signals in dinosaur remains, and environmental gradients of the Late Cretaceous of Montana and Alberta. *Palaeogeogr. Palaeoclimatol. Palaeoecol.* 266, 13–27.
- Galindo, C., Pankhurst, R.J., Casquet, C., Coniglio, J., Baldo, E., Rapela, C.W., Saavedra, J., 1997. Age, Sr- and Nd-isotope systematics, and origin of two fluorite lodes, Sierras Pampeanas, Argentina. *Int. Geol. Rev.* 39, 948–954.
- Ganse, B., Stahn, A., Stoinski, S., Suthau, T., Gunga, H.-C., 2011. Body mass estimation, thermoregulation, and cardiovascular physiology of large sauropods. In: *Biology of the Sauropod Dinosaurs: Understanding the Life of Giants*. Indiana University Press (105–115 pp.).
- Gill, F.L., Hummel, J., Sharifi, A.R., Lee, A.P., Lomax, B.H., 2018. Diets of giants: the nutritional value of sauropod diet during the Mesozoic. *Palaeontology* 61, 647–658.
- Göth, A., 2007. Incubation temperatures and sex ratios in Australian brush-turkey (*Alectura lathami*) mounds. *Austral Ecol.* 32, 378–385.
- Götze, J., 2012. Application of cathodoluminescence microscopy and spectroscopy in geosciences. *Microsc. Microanal.* 18, 1270–1284.
- Grellet-Tinner, G., Fiorelli, L.E., 2010. A new Argentinean nesting site showing neosauropod dinosaur reproduction in a Cretaceous hydrothermal environment. *Nat. Commun.* 1, 1–8.
- Grellet-Tinner, G., Codrea, V., Folie, A., Higa, A., Smith, T., 2012. First evidence of reproductive adaptation to 'island effect' of a dwarf Cretaceous Romanian titanosaur, with embryonic integument in ovo. *PLoS One* 7, e32051.
- Gromet, L.P., Dymek, R.F., Haskin, L.A., Korotev, R.L., 1984. The 'North American shale composite': its compilation, major and trace element characteristics. *Geochim. Cosmochim. Acta* 48, 2469–2482.
- Groscolas, R., Robin, J.P., 2001. Long-term fasting and re-feeding in penguins. *Comp. Biochem. Physiol. A Molecular Integ. Physiol.* 128, 643–653.
- Hechenleitner, E.M., Grellet-Tinner, G., Fiorelli, L.E., 2015. What do giant titanosaur dinosaurs and modern Australasian megapodes have in common? *PeerJ* 3, e1341.
- Hechenleitner, E.M., Grellet-Tinner, G., Foley, M., Fiorelli, L.E., Thompson, M.B., 2016a. Micro-CT scan reveals an unexpected high-volume and interconnected pore network in the Cretaceous Sanagasta dinosaur eggshells. *J. R. Soc. Interface* 13, 20160008.
- Hechenleitner, E.M., Fiorelli, L.E., Grellet-Tinner, G., Leuzinger, L., Basilić, G., Taborda, J.R.A., de la Vega, S.R., Bustamante, C.A., 2016b. A new Upper Cretaceous titanosaur nesting site from La Rioja (NW Argentina), with implications for titanosaur nesting strategies. *Palaeontology* 59, 433–446.
- Hechenleitner, E.M., Fiorelli, L.E., Martinelli, A.G., Grellet-Tinner, G., 2018a. Titanosaur dinosaurs from the Upper Cretaceous of La Rioja province, NW Argentina. *Cretac. Res.* 85, 42–59.
- Hechenleitner, E.M., Taborda, J.R.A., Fiorelli, L.E., Grellet-Tinner, G., Nuñez-Campero, S.R., 2018b. Biomechanical evidence suggests extensive eggshell thinning during incubation in the Sanagasta titanosaur dinosaurs. *PeerJ* 6, e4971.
- Hechenleitner, E.M., Leuzinger, L., Martinelli, A.G., Rocher, S., Fiorelli, L.E., Taborda, J.R.A., Salgado, L., 2020. Two new Late Cretaceous sauropods reveal titanosaur dispersal across South America. *Commun. Biol.* 3, 1–13.
- Hedenquist, J.W., Lowenstern, J.B., 1994. The role of magmas in the formation of hydrothermal ore deposits. *Nature* 370, 519–527.
- Henderson, P., Marlow, C.A., Molleson, T.I., Williams, C.T., 1983. Patterns of chemical change during bone fossilization. *Nature* 306, 358–360.
- Henkes, G.A., Passey, B.H., Grossman, E.L., Shenton, B.J., Pérez-Huerta, A., Yancey, T.E., 2014. Temperature limits for preservation of primary calcite clumped isotope paleotemperatures. *Geochim. Cosmochim. Acta* 139, 362–382.
- Hincke, M.T., Nys, Y., Gautron, J., Mann, K., Rodríguez-Navarro, A.B., Mckee, M.D., 2012. The eggshell: structure, composition and mineralization. *Front. Biosci.* 17, 1266–1280.
- van Hinsbergen, D.J.J., de Groot, L.V., van Schaik, S.J., Spakman, W., Bijl, P.K., Slujs, A., Langereis, C.G., Brinkhuis, H., 2015. A paleolatitude calculator for paleoclimate studies. *PLoS One* 10, 1–21.
- Hobson, K.A., 1995. Reconstructing avian diets using stable-carbon and nitrogen isotope analysis of egg components: patterns of isotopic fractionation and turnover. *Condor* 97, 752–762.
- Hoefs, 2009. *Stable Isotope Geochemistry*. Springer, Berlin Heidelberg (285 pp.).
- Hummel, J., Clauss, M., 2011. Feeding and digestive physiology. In: Klein, N., Remes, K., Gee, C.T., Sander, P.M. (Eds.), *Biology of the Sauropod Dinosaurs: Understanding the Life of Giants*. Indiana University Press, Bloomington, pp. 12–33.
- Iacumini, P., Bocherens, H., Mariotti, A., Longinelli, A., 1996. Oxygen isotope analyses of co-existing carbonate and phosphate in biogenic apatite: a way to monitor diagenetic alteration of bone phosphate? *Earth Planet. Sci. Lett.* 142, 1–6.
- Jackson, S.E., 2008. LAMTRACE data reduction software for LA-ICP-MS. In: *Laser ablation ICP-MS in the Earth sciences: Current practices and outstanding issues*, vol. 40. Mineralogical Association of Canada, pp. 305–307.
- John, C.M., Bowen, D., 2016. Community software for challenging isotope analysis : 642 First applications of "Easotope" to clumped isotopes. *Rapid Commun. Mass Spectrom.* 30, 2285–2300. <https://doi.org/10.1002/rcm.7720>.
- Johnson, B.J., Fogel, M.L., Miller, G.H., 1998. Stable isotopes in modern ostrich eggshell: a calibration for paleoenvironmental applications in semi-arid regions of southern Africa. *Geochim. Cosmochim. Acta* 62, 2451–2461.
- Kele, S., Breitenbach, S.F.M., Capezuoli, E., Meckler, A.N., Ziegler, M., Millan, I.M., Kluge, T., Deak, J., Hanselmann, K., John, C.M., Yan, H., Liu, Z., Bernasconi, S.M., 2015. Temperature dependence of oxygen- and clumped isotope fractionation in carbonates: a study of travertines and tufas in the 6–95°C temperature range. *Geochim. Cosmochim. Acta* 168, 172–192.
- Kelly, J.F., 2000. Stable isotopes of carbon and nitrogen in the study of avian and mammalian trophic ecology. *Can. J. Zool.* 78, 1–27.
- Kim, C.-B., Al-Aasm, I.S., Ghazban, F., Chang, H.-W., 2009. Stable isotopic composition of dinosaur eggshells and pedogenic carbonates in the Upper Cretaceous Seonso Formation, South Korea: paleoenvironmental and diagenetic implications. *Cretac. Res.* 30, 93–99.
- Kim, S.-T., O'neil, J.R., 1997. Equilibrium and nonequilibrium oxygen isotope effects in synthetic carbonates. *Geochim. Cosmochim. Acta* 61, 3461–3475.
- Koch, P.L., 2007. In: Michener, R., Lajtha, K. (Eds.), *Stable isotopes in ecology and environmental science*. Blackwell (566 pp.).
- Koch, P.L., Tuross, N., Fogel, M.L., 1997. The effects of sample treatment and diagenesis on the isotopic integrity of carbonate in biogenic hydroxylapatite. *J. Archaeol. Sci.* 24, 417–429.
- Koch, P.L., Clyde, W.C., Hepple, R.P., Fogel, M.L., Wing, S.L., Zachos, J.C., 2003. Carbon and oxygen isotope records from paleosols spanning the Paleocene–Eocene boundary, Bighorn Basin, Wyoming. *Special Paper Geol. Soc. Am.* 369, 49–64.
- Kocsis, L., Vennemann, T.W., Fontignie, D., 2007. Migration of sharks into freshwater systems during the Miocene and implications for Alpine paleoelevation. *Geology* 35, 451–454.
- Kocsis, L., Trueman, C.N., Palmer, M.R., 2010. Protracted diagenetic alteration of REE contents in fossil bioapatites: direct evidence from Lu-Hf isotope systematics. *Geochim. Cosmochim. Acta* 74, 6077–6092.
- Kohn, M.J., 2010. Carbon isotope compositions of terrestrial C3 plants as indicators of (paleo)ecology and (paleo)climate. *PNAS* 107, 19691–19695.
- Kohn, M.J., Cerling, T.E., 2002. Stable Isotope Compositions of Biological Apatite. 1. In: *Phosphate: Geochemical, Geobiological, and Materials Importance. Mineralogy and Geochemistry*, Vol. 48. Mineralogical Society of America Reviews, pp. 455–488.
- Kuypers, M.M.M., Pancost, R.D., Sinninghe Damsté, J.S., 1999. A large and abrupt fall in atmospheric CO_2 concentration during Cretaceous times. *Nature* 399, 27–30.
- Lacroix, B., Vennemann, T., 2015. Empirical calibration of the oxygen isotope fractionation between quartz and Fe-Mg-chlorite. *Geochim. Cosmochim. Acta* 149, 21–31.
- Lazzerini, N., Lécuyer, C., Amiot, R., Angst, D., Buffetaut, É., Fourel, F., Daux, V., Betancort, J.F., Flandrois, J.-P., Marco, A.S., Lomoschitz, A., 2016. Oxygen isotope fractionation between bird eggshell calcite and body water: application to fossil eggs from Lanzarote (Canary Islands). *Sci. Nature* 103, 1–15.

- Lécuyer, C., Bogey, C., Garcia, J.-P., Granjean, P., Barrat, J.-A., Floquet, M., Bardet, N., Pereda-Superbiola, X., 2003. Stable isotope composition and rare earth element content of vertebrate remains from the Late Cretaceous of northern Spain (Laño): did the environmental record survive? *Palaeogeogr. Palaeoclimatol. Palaeoecol.* 193, 457–471.
- Lécuyer, C., Amiot, R., Touzeau, A., Trotter, J., 2013. Calibration of the phosphate $\delta^{18}\text{O}$ thermometer with carbonate–water oxygen isotope fractionation equations. *Chem. Geol.* 347, 217–226.
- Limarino, C.O., Ciccio, P.I., Krapovickas, K., Benedito, L.D., 2016. Estratigrafía de las sucesiones mesozoicas, paleógenas y neógenas de las quebradas Santo Domingo y el Peñón (Precordillera Septentrional riojana). *Revista de la Asociación Geológica Argentina* 73, 301–318.
- Lindstedt, S.L., Boyce, M.S., 1985. Seasonality, fasting endurance, and body size in mammals. *Am. Nat.* 125, 873–878.
- Luz, B., Kolodny, Y., 1985. Oxygen isotope variations in phosphate of biogenic apatites, IV. Mammal teeth and bones. *Earth Planet. Sci. Lett.* 75, 29–36.
- Luz, B., Kolodny, Y., Horowitz, M., 1984. Fractionation of oxygen isotopes between mammalian bone-phosphate and environmental drinking water. *Geochim. Cosmochim. Acta* 48, 1689–1693.
- Macchioli Grande, M., Alasino, P., Dahlquist, J., Morales Cámara, M., Galindo, C., Basei, M., 2020. Thermal maturation of a complete magmatic plumbing system at the Sierra de Velasco, Northwestern Argentina. *Geol. Mag.* 1–18.
- Mackenzie, K.M., Palmer, M.R., Moore, A., Ibbotson, A.T., Beaumont, W.R.C., Poulter, D. J.S., Trueman, C.N., 2011. Locations of marine animals revealed by carbon isotopes. *Sci. Rep.* 1, 1–6.
- Martínez, F., Parra, M., Arriagada, C., Mora, A., Bascuñán, S., Peña, M., 2017. Late Cretaceous to Cenozoic deformation and exhumation of the Chilean Frontal Cordillera (28°–29°S), Central Andes. *J. Geodyn.* 111, 31–42.
- McCue, M.D., 2013. Comparative Physiology of Fasting, Starvation, and Food Limitation, pp. 1–430.
- McKechnie, A.E., Smit, B., Whitfield, M.C., Noakes, M.J., Talbot, W.A., Garcia, M., Gerson, A.R., Wolf, B.O., McKechnie, A.E., Smit, B., Whitfield, M.C., Noakes, M.J., Talbot, W.A., Garcia, M., 2016. Avian thermoregulation in the heat: evaporative cooling capacity in an archetypal desert specialist, Burchell's sandgrouse (*Pterocles burchelli*). *J. Exp. Biol.* 219, 2137–2144.
- McKibbin, R., Absar, A., Blattner, P., 1986. The transport of oxygen isotopes in hydrothermal systems. In: 8th New Zealand Geothermal Workshop, pp. 29–36.
- Meckler, A.N., Ziegler, M., Millán, M.I., Breitenbach, S.F.M., Bernasconi, S.M., 2014. Long-term performance of the Kiel carbonate device with a new correction scheme for clumped isotope measurements. *Rapid Commun. Mass Spectrom.* 28, 1705–1715.
- Müller, I.A., Fernandez, A., Radke, J., Van Dijk, J., Bowen, D., Schwieters, J., Bernasconi, S.M., 2017. Carbonate clumped isotope analyses with the long-integration dual-inlet (LIDI) workflow: scratching at the lower sample weight boundaries. *Rapid Commun. Mass Spectrom.* 2, 1057–1066.
- Nelson, C.S., Smith, A.M., 1996. Stable oxygen and carbon isotope compositional fields for skeletal and diagenetic components in New Zealand Cenozoic nontropical carbonate sediments and limestones: a synthesis and review. *N. Z. J. Geol. Geophys.* 39, 93–107.
- Nys, Y., Gautron, J., 2007. Structure and Formation of the Eggshell. In: *Bioactive Egg Compounds*. Springer Berlin Heidelberg, Berlin, Heidelberg, pp. 99–102.
- Nys, Y., Guyot, N., 2011. Egg formation and chemistry. In: *Improving the Safety and Quality of Eggs and Egg Products: Egg Chemistry, Production and Consumption*. Woodhead Publishing Limited, pp. 83–132.
- O'Leary, M.H., 1981. Carbon isotope fractionation in plants. *Phytochemistry* 20, 553–567.
- O'Neil, J.R., Roe, L.J., Reinhard, E., Blake, R.E., 1994. A rapid and precise method of oxygen isotope analysis of biogenic phosphate. *Isr. J. Earth Sci.* 43, 203–212.
- Osborne, C.P., Beerling, D.J., 2006. Nature's green revolution: the remarkable evolutionary rise of C4 plants. In: *Philosophical Transactions of the Royal Society of London. Series B, Biological sciences*, vol. 361, pp. 173–194.
- Podlesak, D.W., Torregrossa, A.M., Ehleringer, J.R., Dearing, M.D., Passey, B.H., Cerling, T.E., 2008. Turnover of oxygen and hydrogen isotopes in the body water, CO_2 , hair, and enamel of a small mammal. *Geochim. Cosmochim. Acta* 72, 19–35.
- Pokrovskaya, O.B., Litvin, K.E., Pokrovsky, B.G., 2011. The isotope composition of carbon and oxygen in eggshell of barnacle goose *Branta leucopsis*. *Dokl. Biol. Sci.* 437, 124–127.
- Renner, J.L., White, D.E., Williams, D.L., 1975. Hydrothermal convection systems. In: White, D.E., Williams, D.L. (Eds.), *Assessment of Geothermal Resources of the United States*, Geological Survey Circular, 726. U.S. Geological Survey, pp. 5–57.
- Reynard, B., Lécuyer, C., Grandjean, P., 1999. Crystal-chemical controls on rare-earth element concentrations in fossil biogenic apatites and implications for paleoenvironmental reconstructions. *Chem. Geol.* 155, 233–241.
- Riera, V., Anadón, P., Oms, O., Estrada, R., Maestro, E., 2013. Dinosaur eggshell isotope geochemistry as tools of paleoenvironmental reconstruction for the upper Cretaceous from the Tremp Formation (Southern Pyrenees). *Sediment. Geol.* 294, 356–370.
- Rollinson, H.R., 1993. *Using Geochemical Data: Evaluation, Presentation, Interpretation*. Pearson Education Limited, Essex, England (352 pp.).
- Sander, P.M., Christian, A., Clauss, M., Fehner, R., Gee, C.T., Griebeler, E.M., Gunga, H. C., Hummel, J., Mallison, H., Perry, S.F., Preuschoft, H., Rauhut, O.W.M., Remes, K., Tütken, T., Wings, O., Witzel, U., 2011. Biology of the sauropod dinosaurs: the evolution of gigantism. *Biol. Rev.* 86, 117–155.
- Sarkar, A., Bhattacharya, S.K., Mohabey, D.M., 1991. Stable-isotope analyses of dinosaur eggshells: paleoenvironmental implications. *Geology* 19, 1068–1071.
- Schmid, T.W., Bernasconi, S.M., 2010. An automated method for 'clumped-isotope' measurements on small carbonate samples. *Rapid Commun. Mass Spectrom.* 24, 1955–1963.
- Ségalen, L., Lee-Thorp, J.A., 2009. Palaeoecology of late Early Miocene fauna in the Namib based on $^{13}\text{C}/^{12}\text{C}$ and $^{18}\text{O}/^{16}\text{O}$ ratios of tooth enamel and ratite eggshell carbonate. *Palaeogeogr. Palaeoclimatol. Palaeoecol.* 277, 191–198.
- Sellés, A.G., Vila, B., Galobart, À., 2017. Evidence of reproductive stress in titanosaurian sauropods triggered by an increase in ecological competition. *Sci. Rep.* 7, 1–10.
- Sharp, Z.D., Gibbons, J.A., Maltsev, O., Atudorei, V., Pack, A., Sengupta, S., Shock, E.L., Knauth, L.P., 2016. A calibration of the triple oxygen isotope fractionation in the $\text{SiO}_2\text{-H}_2\text{O}$ system and applications to natural samples. *Geochim. Cosmochim. Acta* 186, 105–119.
- Sheppard, S., 1986. Characterization and isotopic variations in natural waters. *Rev. Mineral.* 16, 165–181.
- Sommer, S.E., 1972. Cathodoluminescence of carbonate, 1. Characterization of cathodoluminescence from carbonate solid solutions. *Chem. Geol.* 9, 257–273.
- de Sosa Tomas, A., Carignano, A.P., Fiorelli, L.E., Hechenleitner, E.M., 2017. Carofitas del Cretácico Tardío de la Formación Los Llanos, La Rioja. Reporte preliminar. In: *V Jornadas de las Ciencias de la Tierra Dr. Eduardo Musacchio*, pp. 34–36.
- Stolper, D.A., Eiler, J.M., 2015. The kinetics of solid-state isotope-exchange reactions for clumped isotopes: a study of inorganic calcites and apatites from natural and experimental samples. *Am. J. Sci.* 315, 363–411.
- Trueman, C.N., Behrensmeier, A.K., Potts, R., Tuross, N., 2006. High-resolution records of location and stratigraphic provenance from the rare earth element composition of fossil bones. *Geochim. Cosmochim. Acta* 70, 4343–4355.
- Tütken, T., 2011. The diet of sauropod dinosaurs - Implications from carbon isotope analyses of teeth, bones, and plants. April. In: Klein, N., Kristian, R., Gee, C.T., Sander, P.M. (Eds.), *Biology of the Sauropod Dinosaurs - Understanding the Life of Giants*. Indiana University Press, pp. 57–79.
- Vennemann, T.W., Fricke, H.C., Blake, R.E., O'Neil, J.R., Colman, A., 2002. Oxygen isotope analyses of phosphates: a comparison of techniques for analysis of Ag_3PO_4 . *Chem. Geol.* 185, 321–336.
- Wang, Y., Cerling, T.E., 1994. A model of fossil tooth and bone diagenesis: implications for paleodiet reconstruction from stable isotopes. *Palaeogeogr. Palaeoclimatol. Palaeoecol.* 107, 281–289.
- White, C.R., Seymour, R.S., 2003. Mammalian basal metabolic rate is proportional to body mass^{2/3}. *Proc. Natl. Acad. Sci. U. S. A.* 100, 4046–4049.
- Williams, D.L.G., Vickers-Rich, P., 1992. Giant fossil egg fragment from the Tertiary of Australia. *Contrib. Sci. Natural History Museum Los Angeles County* 36, 375–378.
- Zazzo, A., Lécuyer, C., Sheppard, S.M.F., Grandjean, P., Mariotti, A., 2004. Diagenesis and the reconstruction of paleoenvironments: a method to restore original $\delta^{18}\text{O}$ values of carbonate and phosphate from fossil tooth enamel. *Geochim. Cosmochim. Acta* 68, 2245–2258.